

Biological control of the chestnut gall wasp with *T. sinensis*: a mathematical model.

Francesco Paparella^{a,*}, Chiara Ferracini^{b,**}, Alessandro Portaluri^b, Alberto Manzo^c, Alberto Alma^b

^a*Division of Sciences - New York University Abu Dhabi - UAE*

^b*Dep. of Agricultural, Forest and Food Sciences - University of Torino - Italy*

^c*Ministry of Agriculture, Food and Forestry - Italy*

Abstract

The Asian chestnut gall wasp *Dryocosmus kuriphilus*, native of China, has become a pest when it appeared in Japan, Korea, and the United States. In Europe it was first found in Italy, in 2002. In 1982 the host-specific parasitoid *Torymus sinensis* was introduced in Japan, in an attempt to achieve a biological control of the pest. After an apparent initial success, the two species seem to have locked in predator-prey cycles of decadal length. We have developed a spatially explicit mathematical model that describes the seasonal time evolution of the adult insect populations, and the competition for finding egg deposition sites. In a spatially homogeneous situation the model reduces to an iterated map for the egg density of the two species. While the map would suggest, for realistic parameters, that both species should become locally extinct (somewhat corroborating the hypothesis of biological control), the full model, for the same parameters, shows that the introduction of *T. sinensis* sparks a traveling wave of the parasitoid population that destroys the pest on its passage. Depending on the value of the diffusion coefficients of the two species, the pest can later be able to re-colonize the empty area left behind the wave. When this occurs the two populations do not seem to attain a state of spatial homogeneity, but produce an ever-changing pattern of traveling waves.

1. Introduction

Since its first report in 2002 the Asian chestnut gall wasp *Dryocosmus kuriphilus* Yasumatsu (Hymenoptera: Cynipidae) is affecting many chestnut ecosystems in Europe and its range is continuously expanding. Native of China,

*Principal corresponding author. Permanent address: Dip. di Matematica & Fisica, Università del Salento, Lecce, Italy.

**Corresponding author.

Email addresses: francesco.paparella@nyu.edu (Francesco Paparella), chiara.ferracini@unito.it (Chiara Ferracini)

it established as a pest in the mid 20th century in several countries, being reported in Japan (1941) (Moriya et al., 2003), in Korea (1958) (Cho and Lee, 1963), in the United States (1974) (Rieske, 2007) in Nepal (1999) (Abe et al., 2007), and in Canada (2012) (Huber and Read, 2012).

In Europe, *D. kuriphilus* was first found in Italy and reported only in 2002 (Brussino et al., 2002). It was added to the European Plant Protection Organization (EPPO) A2 Action list (EPPO, 2005) in 2003. Despite the European Commission Decision 2006/464/EC of 27 June 2006 to put into place provisional emergency measures to prevent the introduction into and the spread within the community of *D. kuriphilus*, the pest is now widely distributed in Italy and has become established in many other European countries including Austria (2013), Croatia (2010), Czech Republic and Slovakia (2012), France (2005), Germany (2013), Hungary (2013), Portugal (2014), Slovenia (2005), Spain (2012), Switzerland (2009), Turkey (2014) and the United Kingdom (2015) (EFSA, 2010; EPPO, 2013, 2015a). In the Netherlands it was accidentally imported through nursery trees (2010) and then promptly detected and eradicated by destroying the few affected plants (NPPO, 2013), but recently a new outbreak has been detected close to the German border (EPPO, 2015b). Since *D. kuriphilus* has shown its ability to spread rapidly and is successfully established in several countries, further establishment is likely in Europe anywhere there is availability of the host plants *Castanea* spp. (EFSA, 2010).

The chestnut gall wasp is a univoltine and thelytokous species (Moriya et al., 1989), and lays eggs in buds during summer. The hatched larvae induce the formation of greenish-red galls, which develop at the time of budburst in the following early spring on new shoots (Ôtake, 1980), suppressing shoot elongation and causing twig dieback. Severe reduction of fruiting with yield losses due to insect attacks have been estimated to reach between 65% and 85% in northern Italy (Bosio et al., 2013; Battisti et al., 2014). However, no evidence was found to confirm tree mortality. A gradual reduction in vigor in the longer term is the likely consequence of annual infestation by the gall wasp, causing a gradual reduction in biomass (EFSA, 2010).

Early attempts of biological control of the pest were performed in Japan (Murakami et al., 1977; Murakami, 1981) and in the USA (Rieske, 2007) by the introduction of *Torymus sinensis* Kamijo (Hymenoptera: Torymidae), a chinese parasitoid described by Kamijo (1982). In its native environment it is only one among many species of natural parasitoids of *D. kuriphilus* (Murakami et al., 1980), but it appears to be very well synchronized with the life cycle of the pest, making it a strong candidate as a biological control agent (Murakami, 1981). In addition, outside China, it was believed to be host-specific, although its host range was never studied or tested in detail (Murakami et al., 1977; Gibbs et al., 2011). Recently, a large-scale survey in northern Italy found a few specimens of *T. sinensis* emerging from oak galls of the non-target host *Biorhiza pallida* Olivier. All evidence, however, still suggests that *D. kuriphilus* is by far the preferred host, and parasitism of other species occurs only exceptionally, possibly as a response to scarcity of its primary host (Ferracini et al., 2015a).

T. sinensis reproduces sexually, and by arrhenotokous parthenogenesis if

there is lack of mating. It is reported as univoltine, like its host. However, recent preliminary investigations highlighted that a very small fraction of the insect population may undergo a prolonged diapause extended for 12 months, mainly as late instar larva (Ferracini et al., 2015b). After emergence, which takes place in early spring, and mating, the female lays eggs inside the larval chamber of newly formed galls, one egg per host larva. Although in controlled conditions occasional multiple eggs per host larva have been reported by an early study (Piao and Moriya, 1992), we have never found more than one egg per host larva while dissecting galls collected in the field. After hatching, the larva feeds ectoparasitically on the host larva, and it pupates in the host larval chamber during winter.

T. sinensis was introduced in Japan from China (Murakami et al., 1977, 1980; Moriya et al., 2003). After its release, it dispersed successfully alongside expanding *D. kuriphilus* populations. In Japan *D. kuriphilus* may also be subject to varying levels of parasitism from native insects, most notably *Torymus beneficus* Yasumatsu & Kamijo and several species of the genus *Eupelmus* (Murakami and Gyoutoku, 1995; Moriya et al., 2003) that, however, are unable to control the pest. Monitoring of test orchards showed that after about 6–18 years from the introduction of *T. sinensis*, the pest population declined to levels as low as to be practically undetectable, giving rise to claims of success in biologically controlling the infestation (Moriya et al., 1989; Murakami et al., 2001; Moriya et al., 2003). However, continuous monitoring of the first release site over 25 years shows three successive peaks in the population of *D. kuriphilus*, shortly followed by peaks in the population of *T. sinensis* (Moriya, personal communication). In the USA, several Asian *Torymus* species were released in 1977 in southeastern Georgia, but the release was not followed by any monitoring. The first accounts of the successful establishment of *T. sinensis* in the United States were published only thirty years later (Cooper and Rieske, 2007; Rieske, 2007). In spite of the abundant presence of *T. sinensis*, and of *Ormyrus labotus* Walker (a native insect that was shown to easily parasitize *D. kuriphilus* galls), the pest could be found in most of the southern Appalachian range, with satellite infestations in Ohio and Pennsylvania.

The European chestnut (*Castanea sativa* Mill.) is one of the most important broad-leaved species in Italy: chestnut stands amount to 788,400 hectares, which represents 9% of the Italian forests (Graziosi and Santi, 2008). Due to the report of the gall wasp in 2002 and in consideration of the long-established economic importance of chestnut throughout the country for fruit and wood production, a collaboration was started with Japanese researchers and a biological control program was initiated in 2005 with the release in infested orchards of Japan-imported *T. sinensis* specimens (Quacchia et al., 2008). Following the Japanese and Italian experiences, reporting the establishment of a sizable population of *T. sinensis* vigorously parasitizing the galls of *D. kuriphilus*, recent releasing programs were performed in Croatia, France and Hungary (Borowiec et al., 2014; Matošević et al., 2014), as well as test releases in Spain and Portugal (Associação Portuguesa da Castanha, personal communication).

Although in Europe there exist several native species of Hymenoptera capa-

ble of parasitizing *D. kuriphilus* galls, all of them have a very large host range, and suffer by a mismatch between their emergence times and the development of the galls. They are therefore unable to act effectively as biological control agents (Quacchia et al., 2013; Alma et al., 2014).

In the present paper we develop a mathematical model of the interaction between *T. sinensis* and *D. kuriphilus*, aiming at developing a tool for understanding and evaluating the effectiveness of biological control programs based on the release of *T. sinensis* in woods and orchards infested by *D. kuriphilus*.

In particular we would like to investigate whether *T. sinensis* should be expected to be able, alone, to cause the local extinction of *D. kuriphilus*, or maintain its population to levels as low as to produce no harm, or if such expectations are over optimistic. The fact that *T. sinensis* is extremely well synchronized with *D. kuriphilus*, that outside China it acts almost perfectly as host-specific, and that in Europe its abundance appears to be limited only by the availability of its host, with a very low mortality during all its life stages, allows hopes for a rapid, complete, and permanent control of the pest. However, the experiences of both Japan and the USA warn that the effectiveness of *T. sinensis* might be less perfect than one would wish it to be. In the case of Japan the imperfect control of *D. kuriphilus* has been ascribed to a high mortality of *T. sinensis* by hyperparasitism (Murakami and Gyoutoku, 1991). In Europe hyperparasitism is only occasional (Quacchia et al., 2013), which leaves more room for hopes of obtaining a control.

In order to have a flexible tool, our model, in its full form, is a spatially-explicit one, which also explicitly describes, both for *T. sinensis* and for *D. kuriphilus*, the seasonal time evolution of the adult insect population, and the competition for finding the egg deposition sites. In a spatially-homogeneous situation the model may be rigorously reduced to an iterated map quantifying the egg density of the two species, whose properties are studied with a combination of analytic and numerical techniques. The full, spatially-explicit model is studied by means of numerical simulations in one and two spatial dimensions. The comparison between the dynamics of the iterated maps and of the full model suggests a diffusion-based mechanisms that may give rise, under certain conditions, to repeated waves of full infestation followed by near disappearance of the pest and of its parasitoid, on time scales that depend non only on the physiological and ecological parameters, but also on the size and geometry of the wood.

The rest of the paper is organized as follows: the mathematical model is developed in section 2; the results obtained from the model are reported in detail in section 3; finally they are summarized in section 4, together with some speculative considerations. Section 5 is an appendix containing mathematical analyses in support of statements appearing in sections 2 and 4.

2. The model

2.1. Equations for the gall wasp

We describe the population of adult gall wasps during the summer of the year n as a field U_n quantifying the density (that is, number of insects per unit area) of egg-carrying *D. kuriphilus* adults. By “density of egg-carrying adults” we mean that an adult that has not yet laid any eggs contributes by a whole unit in the computation of this density, an adult that has laid, say, half its eggs contributes by half a unit, and one that has laid all its eggs does not contribute at all, even if it is still alive. Thus, calling N_D the maximum number of eggs that can be laid by a typical *D. kuriphilus* adult under optimal conditions, then $N_D U_n(\mathbf{x}, t)$ is the number of eggs per unit area present at the location \mathbf{x} and time t that can still potentially be laid.

We shall also need a second field, V_n , that quantifies the density of eggs laid in chestnut buds. Because *D. kuriphilus* may only lay eggs on chestnuts buds, and at most M eggs per bud, then the density of laid eggs in any location \mathbf{x} is always at most $M\beta_n(\mathbf{x})$, where β_n is the density of chestnut buds on the n -th year. In any case, the maximum density of laid eggs cannot exceed the quantity

$$V_{max} = M\beta_{max} \quad (1)$$

where the constant β_{max} is the maximum density of buds attainable in a chestnut wood under optimal conditions.

At the beginning of each season, the density of both the gall wasps and of their laid eggs are zero:

$$\begin{cases} U_n(\mathbf{x}, 0) &= 0 \\ V_n(\mathbf{x}, 0) &= 0 \end{cases} \quad (2)$$

As the season progresses, from the galls formed during the previous season, the wasps gradually emerge. For simplicity we shall assume a constant emergence rate:

$$\text{emergence rate} = \frac{\eta V_{n-1}(\mathbf{x}, T_D)}{T_D} \quad (3)$$

where T_D is the length of the egg deposition season, and the non-dimensional parameter $\eta \in (0, 1]$ is the survival rate during the overwintering. More precisely, $\eta V_{n-1}(\mathbf{x}, T_D) dA$ is the number of *D. kuriphilus* adults that emerge during the n -th season from an area dA centered around the location \mathbf{x} . Taking into account that chestnut gall wasps reproduce by thelytokous parthenogenesis (Murakami, 1981), and have a low natural mortality of eggs and larvae, we expect the numerical value of η to be close to one. More in detail, the primary mortality factors for *D. kuriphilus* are parasitism, gall-chamber invading fungi and failure of adult gall wasp to emerge (Cooper and Rieske, 2010), but from our experience all these processes have effects so mild to be almost negligible (authors’ personal observation).

Individual gall wasps do not survive for more than a few days. Therefore we need to introduce a sink term representing their mortality rate. We are not

aware of any evidence in the literature of important exogenous factors affecting the mortality of adult gall wasps. Thus, taking individual deaths as independent from each other, the rate of deaths per unit area is likely to be proportional to the density of the population, suggesting the following simple choice for the death rate term

$$\text{death rate} = -\frac{U_n(\mathbf{x}, t)}{a} \quad (4)$$

where a is the typical adult life span (up to ten days: EFSA, 2010).

We shall assume that during the egg-laying season the gall wasps move randomly, diffusing isotropically in the forest. Although there is evidence of a response of *D. kuriphilus* to olfactory cues in the choice of a host twig, this was observed spatial scales shorter than a meter (Germinara et al., 2011). On much larger scales there is no evidence of anisotropic motion of the gall wasps, nor it should be expected. Following olfactory cues in a turbulent environment, such as a wood canopy, is a very challenging task when there is a single odor source (Balkowsky and Shraiman, 2002). In the presence of multiple sources it is very unlikely that an insect can consistently and reliably exploit olfactory cues on long range. For example, in the case of the parasitoid wasp *Diachasmimorpha juglandis* Muesebeck, it was verified that it preferred to use visual cues rather than olfactory ones for locating the walnut fruit husks where its host may be found (Henneman et al., 2002). In the case of *D. kuriphilus*, the available visual cues are also short-range: chestnut buds are not visible from more than a few meters away. Therefore, we consider reasonable to assume that the large-scale motion (that is, on distances larger than the size of individual trees) of *D. kuriphilus* adults is aimless and random, and thus it should be modeled by a Laplacian diffusion operator (we shall further discuss this issue in section 4).

When the egg-carrying adults find available buds (that is buds that are not already fully saturated by other eggs), they quickly lay one or more eggs, thus reducing the number of available deposition sites. The rate of egg deposition of an individual will be proportional to the density of available eggs deposition sites, which, in the model, is expressed as $M\beta_n(\mathbf{x}) - V_n(\mathbf{x}, t)$. It would be more accurate to assume that the egg deposition rate is a Holling's type II function of the available egg deposition sites. However, our observations suggest that, for *D. kuriphilus*, the handling time (the time actually spent laying eggs) is just a tiny fraction of the search time (which is comparable with the adult life span). When the handling time is negligible, the Holling's type II function tends to a simple proportionality between the deposition rate and the density of available deposition places (see e.g. Vandermeer and Goldberg, 2013, p.163). Accordingly, the egg deposition rate of the whole population is taken as proportional to the product of the density of available sites by the density of the adult population, as in the following expression

$$\text{egg deposition rate} = r_D \frac{M\beta_n(\mathbf{x}) - V_n(\mathbf{x}, t)}{V_{max}} U_n(\mathbf{x}, t). \quad (5)$$

It is possible to give a reasonable estimate for the proportionality constant r_D that appears in the expression above. In fact, we must assume that in optimal

conditions (that is, if $V_n = 0$, $\beta_n(\mathbf{x}) = \beta_{max}$ and thus the deposition rate reduces to $r_D U_n$) every adult gall wasp must be able to lay all its N_D eggs in a time interval roughly equal to its adult life span a . This would imply that

$$r_D = \frac{N_D}{a} \quad (6)$$

By adding together all the processes discussed in this section we arrive to the following model that describes the time evolution of the U_n and V_n fields during the n -th season.

$$\left\{ \begin{array}{l} \frac{\partial}{\partial t} U_n(\mathbf{x}, t) = D_D \nabla^2 U_n(\mathbf{x}, t) - \frac{1}{a} \frac{M\beta_n(\mathbf{x}) - V_n(\mathbf{x}, t)}{V_{max}} U_n(\mathbf{x}, t) \\ \quad - \frac{1}{a} U_n(\mathbf{x}, t) + \frac{\eta V_{n-1}(\mathbf{x}, T_D)}{T_D} \\ \frac{\partial}{\partial t} V_n(\mathbf{x}, t) = \frac{N_D}{a} \frac{M\beta_n(\mathbf{x}) - V_n(\mathbf{x}, t)}{V_{max}} U_n(\mathbf{x}, t) \end{array} \right. \quad (7)$$

where D_D is the diffusivity of the gall wasps, and all other symbols have already been defined. Note that the egg deposition rate, that appears as the only term in the right-hand side of the equation for V_n , also appears in the equation for U_n with a minus sign and divided by N_D . This is because, as discussed above, the contribution of each individual to the density U_n is weighted by the fraction of eggs that it carries.

The problem (7) with the initial conditions (2) is not closed, because no rule was specified for the time evolution of the bud density β_n . In the presence of a developed infestation the health of the chestnut trees progressively deteriorates, and the bud density may decrease. This is a slow process, whose details are largely unknown (Kato and Hijii, 1997). If the model were used to perform detailed, realistic year-by-year forecasts of the spreading of *D. kuriphilus*, the best results would be obtained by measuring the density β_n by means of direct surveys of the orchards and coppices under study. In this paper, in order to assess and understand the main features of the solutions of the model's equations, we shall use the strong simplifying assumption that the density of buds is always constant, and equal to β_{max} .

It is convenient to make non-dimensional the dependent variables, by defining $u_n = U_n/(\eta V_{max})$ and $v_n = V_n/V_{max}$. Note that $v_n \in [0, 1]$ and that $M\beta_n/V_{max} = 1$, because of the simplifying assumption $\beta_n = \beta_{max}$. Likewise, it is convenient to use non-dimensional variables also for time and space. These are defined as: $\tilde{t} = t/T_D$ and $\tilde{\mathbf{x}} = \mathbf{x}/\sqrt{D_D T_D}$. Thus the equations (7) become (for typographical brevity in the following we shall omit the tildes on the non-dimensional independent variables)

$$\left\{ \begin{array}{l} \frac{\partial}{\partial \tilde{t}} u_n(\mathbf{x}, t) = \nabla^2 u_n(\mathbf{x}, t) - \mu(2 - v_n(\mathbf{x}, t)) u_n(\mathbf{x}, t) + v_{n-1}(\mathbf{x}, 1) \\ \frac{\partial}{\partial \tilde{t}} v_n(\mathbf{x}, t) = E_D \mu(1 - v_n(\mathbf{x}, t)) u_n(\mathbf{x}, t) \end{array} \right. \quad (8)$$

where $\mu = T_D/a$, $E_D = \eta N_D$ and $t \in [0, 1]$. For each n , the equations (8) are subject to the conditions

$$\begin{cases} u_n(\mathbf{x}, 0) &= 0 \\ v_n(\mathbf{x}, 0) &= 0 \end{cases} \quad (9)$$

This is a piecewise smooth initial value problem, characterized by two free parameters: E_D and μ . The first one is the maximum number of eggs that can be laid by a *D. kuriphilus* adult, multiplied by the overwintering mortality (which does not appear elsewhere in the non-dimensional equations); the second is the reciprocal of the adult life span, measured in the non-dimensional time units. A further important parameter is the size, in non-dimensional units, of the domain Ω , that is the chestnut-covered area on which U_n and V_n are defined. The equations (8) and the conditions (9) must be complemented by suitable boundary conditions describing the behavior of the gall wasps when they find themselves at the edge of the wood. We are not aware of any published work on this issue. It is very likely that a small fraction of the gall wasps would venture outside a chestnut orchard or coppice, spilling over adjacent regions. For simplicity, here we assume that any gall-wasp that were to leave the domain Ω would promptly change its course, returning inside the chestnut-populated area. In this idealized situation there would be no flux of wasps across the edges of Ω , and therefore the appropriate boundary conditions for U_n would be

$$\hat{\mathbf{n}} \cdot \nabla u_n|_{\partial\Omega} = 0 \quad (10)$$

where $\partial\Omega$ denotes the line delimiting the boundary of Ω , and $\hat{\mathbf{n}}$ represents the outward unit vector perpendicular to $\partial\Omega$.

The no-flux boundary condition (10) is of particular interest because it allows for homogeneous solutions, that is, solutions in which the densities u_n and v_n are constant in space (but not in time). In particular, it is straightforward to verify that if s_0 is taken as a constant, then at all later times t and seasons n , u_n and v_n do not depend on \mathbf{x} , and the problem (8,9,10) reduces to the following chain of ordinary differential equations:

$$\begin{cases} \dot{u}_n(t) &= v_{n-1}(1) - \mu(2 - v_n(t))u_n(t) \\ \dot{v}_n(t) &= E_D\mu(1 - v_n(t))u_n(t) \\ u_n(0) &= 0 \\ v_n(0) &= 0 \end{cases} \quad (11)$$

where the dot denotes differentiation with respect to time. The solution of these nonlinear equations cannot be expressed in terms of simple functions. However, a formal calculation shows that the year-over-year dynamics of the egg density can be well approximated by the following simple map (see Appendix 5.1 for details)

$$v_n = 1 - e^{-kv_{n-1}} \quad (12)$$

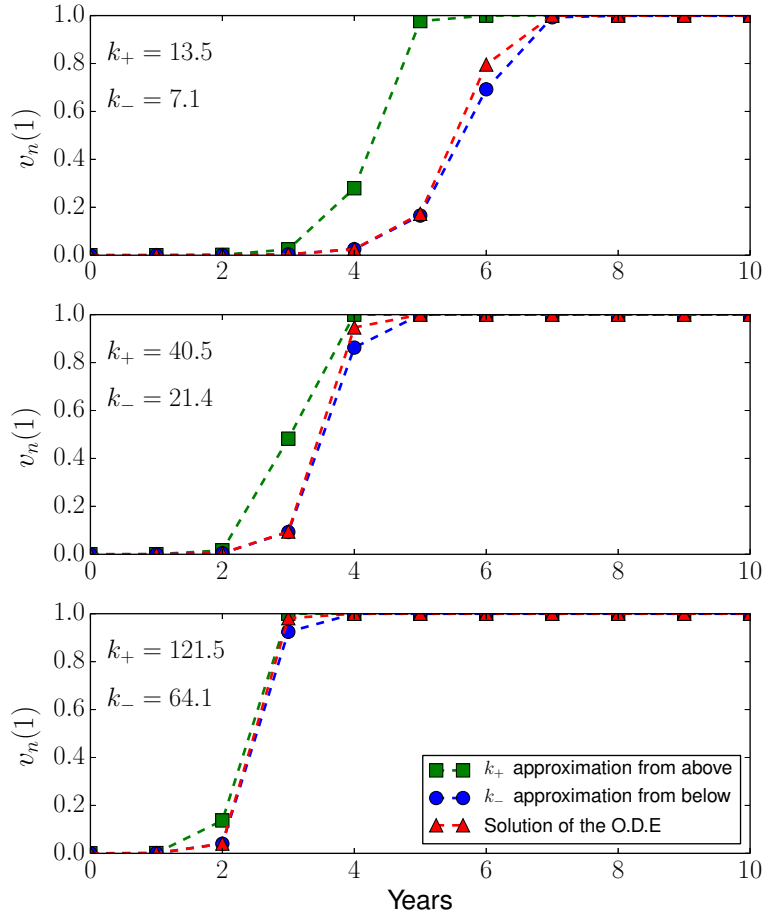


Figure 1: Comparison of the end-of-season egg densities given by Skellam's map (12) and by a numerical solution of the spatially-homogeneous model (11) for different values of the parameter k_{\pm} defined in (13). In all the computations we have used $N_D = 150$, $\mu = 10$, $v_0(1) = 10^{-5}$. The overwintering survival rates are, from top to bottom, $\eta = 0.1, 0.3, 0.9$. The first two values are unrealistically low and are meant just to illustrate the properties of the two approximations. The last value is considered to be realistic in the European setting.

where the egg densities v_n, v_{n-1} are evaluated at time $t = 1$ (corresponding to the end of the n -th and $(n - 1)$ -th seasons). The positive constant k that appears in the exponential is given by one of the following two expressions

$$\begin{cases} k_+ = \frac{E_D}{\mu} (e^{-\mu} + \mu - 1) & \text{approx. from above,} \\ k_- = \frac{E_D}{4\mu} (e^{-2\mu} + 2\mu - 1) & \text{approx. from below.} \end{cases} \quad (13)$$

On choosing $k = k_-$ we obtain an approximation from below, which is highly accurate when the previous year egg density v_{n-1} is appreciably smaller than 1. Choosing $k = k_+$ one has an approximation from above, that captures the dynamics more accurately when the egg density v_{n-1} is close to 1. (see Appendix 5.1 for details, and Figure 1).

We observe that the iterated map (12) is the well-known model of Skellam (Skellam, 1951; Brännström and Sumpter, 2005), that describes the population dynamics of univoltine insects in a regime of contest competition.

2.2. Equations for *T. sinensis*

Torymus adults emerge from vacated galls in spring. There appears to be a good degree of synchronism in the emergence process, so that the great majority of all the individuals appear in a time span of a few days (authors' personal observation). After mating, the egg-carrying females look for intact galls into which they lay (usually) one egg per chamber (Piao and Moriya, 1992). Each female initially carries about $N_T \approx 70$ eggs. In outdoor conditions the adult lifetime of *T. sinensis* is at least 37 days (Piao and Moriya, 1992). For modeling purposes we shall take the emergence as an instantaneous process, and attribute the same life-span to all the individuals, so that they all die together.

In the following we will denote with P_n the density of the egg-carrying *T. sinensis* females and with Q_n the density of the eggs already laid, during the n -th season. Just as in our model of *D. kuriphilus*, we shall use the following expression for the egg deposition rate of *T. sinensis*

$$\text{egg deposition rate} = r_T \frac{\eta V_{n-1}(\mathbf{x}, T_D) - Q_n(\mathbf{x}, t)}{V_{max}} P_n(\mathbf{x}, t) \quad (14)$$

Also in this case, in principle, the rate should be expressed through a Holling's type II functional response. But the oviposition time of *T. sinensis* is very short (a few minutes, authors' personal observation) in comparison with its search time. Thus, as we argued in the case of the gall wasp, the deposition rate must be proportional to the product of the density of egg-carrying *T. sinensis* females with the density of the sites where oviposition is possible. The latter is given by the difference between the density of gall wasp eggs laid during the previous season and turned into larvae (namely ηV_{n-1}) and the density of *T. sinensis* eggs already laid. Here r_T/V_{max} is the proportionality constant. As for the gall-wasp we should assume that every female *Torymus*, in optimal conditions (that is, $\eta V_{n-1} = V_{max}$ and $Q_n = 0$), should be able to lay all its N_T eggs during its life span T_T . Thus, we assume

$$r_T = \frac{N_T}{T_T}. \quad (15)$$

Also for *T. sinensis* it is known that it responds to olfactory and visual cues at short ranges (Graziosi and Rieske, 2013). On longer distances, the same considerations already mentioned for the gall-wasp apply: the overall motion of an adult *T. sinensis* during its life span should be random and aimless, and therefore a Laplacian diffusion process, characterized by a constant diffusivity D_T , should be the appropriate model.

Therefore we may describe the dynamics of a population of *T. sinensis* during the n -th season with the following equations:

$$\begin{cases} \frac{\partial}{\partial t} P_n(\mathbf{x}, t) &= D_T \nabla^2 P_n(\mathbf{x}, t) - \frac{1}{T_T} \frac{\eta V_{n-1}(\mathbf{x}, T_D) - Q_n(\mathbf{x}, t)}{V_{max}} P_n(\mathbf{x}, t) \\ \frac{\partial}{\partial t} Q_n(\mathbf{x}, t) &= \frac{N_T \eta V_{n-1}(\mathbf{x}, T_D) - Q_n(\mathbf{x}, t)}{T_T V_{max}} P_n(\mathbf{x}, t) \end{cases}. \quad (16)$$

Here the time $t = 0$ corresponds to the simultaneous emergence of the adult *Torymus*. The equations are valid up to $t = T_T$, corresponding to the end of the *Torymus* season, when all the adults die. Just as we did for the gall wasp, the rate of change of the laid egg density Q_n is equal to the egg deposition rate. This rate is also divided by N_T and subtracted from the equation for the rate of change of the density P_n of the *T. sinensis* females, because the density of adult females is weighted by the number of eggs that each adult carries.

The equations (16) are subject to the initial conditions

$$\begin{cases} P_n(\mathbf{x}, 0) &= \gamma Q_{n-1}(\mathbf{x}, T_T) \\ Q_n(\mathbf{x}, 0) &= 0 \end{cases} \quad (17)$$

The initial density of *T. sinensis* females is not zero because we assumed the instantaneous emergence of all the adults. The constant γ accounts for the sex ratio of *T. sinensis*, and for the mortality rate of the overwintering larvae. Male and female have roughly the same probability to emerge from a fertilized egg of *T. sinensis* (Ferracini et al., 2015b) and the overwintering mortality is believed to be very low (author's personal observation), thus we shall use values of γ smaller than, but close to 1/2. *T. sinensis* females that are not able to mate may still lay their unfertilized eggs, from which will emerge males, by arrhenotokous parthenogenesis. Therefore, if the density of *T. sinensis* drops to very low levels, in the next season the sex ratio will be skewed in favor of the males, resulting in an improved mating probability for the remaining females. In its present form, our model does not include this mechanism. However, we also do not model explicitly the mating process: all the females are implicitly considered to be fertilized at the moment of their emergence. Thus we are already overestimating the mating probability of the females, and we feel that, at this stage, further complications may be unnecessary. For the same reason, *T. sinensis* is modeled as a strictly univoltine species. The recent observations of an extended diapause of a few *Torymus* individuals, in a controlled setting (Ferracini et al., 2015b), does not yet allow a quantitative assessment of the importance (if any) of this process for the dynamics of the population in the

wild. Thus we postpone the inclusion of these processes for a possible future improved version of the model.

It is convenient to rewrite the model by using the non-dimensional densities $p_n = P_n/(\gamma\eta V_{max})$, $q_n = Q_n/(\eta V_{max})$, and the same non-dimensional space and time variables already used for the gall-wasp equations. The equations (16) then become

$$\begin{cases} \frac{\partial}{\partial t} p_n(\mathbf{x}, t) = \delta \nabla^2 p_n(\mathbf{x}, t) - \tau^{-1} (v_{n-1}(\mathbf{x}, 1) - q_n(\mathbf{x}, t)) p_n(\mathbf{x}, t), \\ \frac{\partial}{\partial t} q_n(\mathbf{x}, t) = E_T \tau^{-1} (v_{n-1}(\mathbf{x}, 1) - q_n(\mathbf{x}, t)) p_n(\mathbf{x}, t), \end{cases} \quad (18)$$

where we have defined the diffusivity ratio $\delta = D_T/D_D$, the non-dimensional *T. sinensis* season length $\tau = T_T/(\eta T_D)$, and the effective egg number $E_T = \gamma N_T$. The initial conditions (17) become

$$\begin{cases} p_n(\mathbf{x}, 0) = q_{n-1}(\mathbf{x}, \eta\tau), \\ q_n(\mathbf{x}, 0) = 0. \end{cases} \quad (19)$$

By imposing no-flux boundary conditions on p_n , and looking for homogeneous solutions, the equations (18) together with the initial conditions, yield a set of ordinary differential equations whose solution is given in Appendix (5.2). By evaluating the solution at the time corresponding to the end of the *Torymus* season, that is at the non-dimensional time $t = \eta\tau$, we obtain the following map:

$$q_{n+1} = \begin{cases} \frac{E_T v_n q_n (1 - e^{\eta(E_T q_n - v_n)})}{v_n^2 - E_T q_n e^{\eta(E_T q_n - v_n)}}, & E_T q_n \neq v_n \\ \frac{v_n^2}{v_n + \eta^{-1}}, & E_T q_n = v_n \end{cases} \quad (20)$$

where the egg densities q_{n+1} , q_n and v_n are evaluated at the end of their respective seasons. Albeit complicated-looking, the right-hand side of the map is a smooth function of its parameters, even for $E_T q_n = v_n$. In particular, it is a growing function of q_n , and, for realistic values of E_T and η , it rapidly approaches the horizontal asymptote $q_{n+1} \rightarrow v_n$. Therefore, the map (20), and thus the underlying equations (16), are a model that describes a contest competition process among the individuals of *T. sinensis* (Brännström and Sumpter, 2005).

2.3. The complete model

The equations for *T. sinensis*, discussed in the previous subsection, already depend on the density of *D. kuriphilus* eggs laid in the previous year. In order to have a fully coupled model, we only need to incorporate the parasitism of *T. sinensis* in the equations for *D. kuriphilus* discussed in sec 2.1. This is easily accomplished by observing that parasitized larvae of *D. kuriphilus* simply won't give rise to adults. Therefore we need to change the emergence rate (3) with

$$\text{emergence rate} = \frac{\eta V_{n-1}(\mathbf{x}, T_D) - Q_n(\mathbf{x}, T_T)}{T_D}. \quad (21)$$

The complete model, using the non-dimensional variables, then reads

$$\left\{ \begin{array}{l} \frac{\partial}{\partial t} p_n(\mathbf{x}, t) = \delta \nabla^2 p_n(\mathbf{x}, t) - \tau^{-1} (v_{n-1}(\mathbf{x}, 1) - q_n(\mathbf{x}, t)) p_n(\mathbf{x}, t) \\ \frac{\partial}{\partial t} q_n(\mathbf{x}, t) = E_T \tau^{-1} (v_{n-1}(\mathbf{x}, 1) - q_n(\mathbf{x}, t)) p_n(\mathbf{x}, t) \\ \frac{\partial}{\partial t} u_n(\mathbf{x}, t) = \nabla^2 u_n(\mathbf{x}, t) - \mu (2 - v_n(\mathbf{x}, t)) u_n(\mathbf{x}, t) + v_{n-1}(\mathbf{x}, 1) - q_n(\mathbf{x}, \eta \tau) \\ \frac{\partial}{\partial t} v_n(\mathbf{x}, t) = E_D \mu (1 - v_n(\mathbf{x}, t)) u_n(\mathbf{x}, t) \\ p_n(\mathbf{x}, 0) = q_{n-1}(\mathbf{x}, \eta \tau) \\ q_n(\mathbf{x}, 0) = 0 \\ u_n(\mathbf{x}, 0) = 0 \\ v_n(\mathbf{x}, 0) = 0. \end{array} \right. \quad (22)$$

In the case of space-independent solutions, the dynamic of this model is well approximated by the following map

$$\left\{ \begin{array}{l} q_{n+1} = \begin{cases} \frac{E_T v_n q_n (1 - e^{\eta(E_T q_n - v_n)})}{v_n^2 - E_T q_n e^{\eta(E_T q_n - v_n)}}, & E_T q_n \neq v_n \\ \frac{v_n^2}{v_n + \eta^{-1}}, & E_T q_n = v_n \end{cases} \\ v_{n+1} = 1 - e^{-k(v_n - q_{n+1})} \end{array} \right. \quad (23)$$

that describes the year-over-year change of the end-of-season density of *T. sinensis* and *D. kuriphilus* eggs.

2.4. The value of the parameters

The mathematical model developed in this section depends on 11 free parameters, listed in Table 1. Of these, one depends on the physiology and on the distribution of the chestnuts, namely the bud density β_{max} . Its numerical value and its significance will be discussed at the beginning of the next section.

The other 10 parameters are related to the physiology of either *D. kuriphilus* or to *T. sinensis*. The value of 6 of these, namely M , a , T_D , T_T , N_D , N_T , is fairly well-known; the value of η and γ is debatable, and it might be different in different regions of the world; the value of D_D and D_T is unknown, but the model links it to more readily measurable quantities. We shall now briefly discuss all of them in turn.

The maximum number M of eggs of *D. kuriphilus* per chestnut bud is only used in the definition of the non-dimensional densities (see Table 2) but it does not enter in the parameters that appear in the non-dimensional model (22). Thus, any uncertainty in its value would not affect the dynamics. Then there are three intervals of time: the life span a of adult individuals of *D. kuriphilus*; the number of days T_D during which the adults of *D. kuriphilus* are active (that is, the length of what we have called the “*Dryocosmus* season”); and the number of days T_T during which the adults of *T. sinensis* are active (the “*Torymus* season”). What matters for the model are the non-dimensional ratios T_D/a and

D_D	$0.77 \text{ km}^2 \text{ d}^{-1}$	Diffusion coefficient of <i>D. kuriphilus</i> .	See sec. 3.2.
a	2–10 days 2–3 days	Adult life span of <i>D. kuriphilus</i> .	EFSA (2010); Graziosi and Rieske (2014).
M	20–30 eggs bud ⁻¹	number of eggs of <i>D. kuriphilus</i> that can be laid on a bud.	EFSA (2010).
β_{max}	$2 \cdot 10^6$ buds ha ⁻¹	Maximum density of chestnut buds.	Bounous (2014).
η	0.5–0.98	Fraction of <i>D. kuriphilus</i> larvae surviving after overwintering.	Cooper and Rieske (2007); Quacchia et al. (2013).
T_D	30–50 days	Length of the egg deposition season for <i>D. kuriphilus</i> .	EPPO (2005).
N_D	100–300	Number of eggs per adult of <i>D. kuriphilus</i> .	Graziosi and Rieske (2014).
D_T	unknown	Diffusion coefficient of <i>T. sinensis</i> .	See sec. 3.3
T_T	37 days or more	Length of the egg deposition season for <i>T. sinensis</i> .	Piao and Moriya (1992).
N_T	71	Number of eggs per adult female of <i>T. sinensis</i> .	Piao and Moriya (1992).
γ	0.25–0.45	Fraction of <i>T. sinensis</i> larvae that are female and survive after overwintering.	Piao and Moriya (1992) Author's unpublished observations

Table 1: Parameters of the model and their likely value or value range.

$u_n = \frac{U_n}{\eta M \beta_{max}}$	Non-dimensional density of <i>D. kuriphilus</i> adults during the season n .
$v_n = \frac{V_n}{M \beta_{max}}$	Non-dimensional density of <i>D. kuriphilus</i> eggs laid during the season n .
$p_n = \frac{P_n}{\gamma \eta M \beta_{max}}$	Non-dimensional density of <i>T. sinensis</i> adult females during the season n .
$q_n = \frac{Q_n}{\eta M \beta_{max}}$	Non-dimensional density of <i>T. sinensis</i> eggs laid during the season n .
$\mu = \frac{T_D}{a}$	Non-dimensional length of the egg deposition season of <i>D. kuriphilus</i> .
$E_D = \eta N_D$	Number of larvae per adult of <i>D. kuriphilus</i> that survive the overwintering in optimal conditions.
$k = \begin{cases} k_+ = \frac{E_D}{\mu} (e^{-\mu} + \mu - 1) \\ k_- = \frac{E_D}{4\mu} (e^{-2\mu} + 2\mu - 1) \end{cases}$	Effective growth rate in the Skellam maps approximating from above ($k = k_+$) or from below ($k = k_-$) the year-over-year dynamics of <i>D. kuriphilus</i> ' egg density.
$\delta = \frac{D_T}{D_D}$	Diffusivity ratio.
$\tau = \frac{T_T}{\eta T_D}$	Non-dimensional length of the egg deposition season of <i>T. sinensis</i> .
$E_T = \gamma N_T$	Number of female larvae per adult female of <i>T. sinensis</i> that survive the overwintering in optimal conditions.

Table 2: Non-dimensional variables and parameters. Here the unit of time is T_D and the unit of space is $\sqrt{D_D T_D}$.

T_T/T_D . We take 10 as the reference value for the first, and 1 for the second. We have verified that any discrepancy from these reference values, as long as it is compatible with the observational uncertainties, makes little difference in the end results. In particular, in the spatially homogeneous case, the calculations of the previous section show that the map (23) does not depend on their ratio. Finally we have N_D and N_T , respectively the average number of eggs carried by *D. kuriphilus* and *T. sinensis* females. For the first we take the reference value of 150 eggs per female, and for the second we take 70 eggs per female. In the non-dimensional model (22) these parameters always appear multiplied, respectively, by η and γ . Any uncertainty in the value of N_D and N_T is surely swamped by the uncertainty in these two parameters.

In fact, the value of the two overwintering survival fractions η (of *D. kuriphilus*) and γ (of *T. sinensis*, which also includes the sex ratio) are debatable. The works of Cooper and Rieske (2007) and of Piao and Moriya (1992) suggest intermediate values for these parameters. However, our own observations (published in Quacchia et al., 2013 for *D. kuriphilus* and yet unpublished for *T. sinensis*) suggest much higher survival fractions. Whether these discrepancies are due to regional variations (USA and Japan vs subalpine Europe) or to some other cause is, at present, not known. Therefore, in the following, we devote much attention to studying the dependence of the dynamics on the value of the overwintering survival fractions.

The two diffusion coefficients D_D and D_T , respectively of *D. kuriphilus* and *T. sinensis*, are completely unknown. In §3.2 we estimate the value of D_D on the basis of the model results and of the observed speed with which a population of *D. kuriphilus* is able to invade a chestnut forest. Not enough data are available for attempting a similar deduction with D_T . The effect of changing the diffusivity is studied in detail in §3.3.

3. Results

3.1. Space-independent dynamics

The map (23), which describes the time evolution of spatially homogeneous populations of *D. kuriphilus* parasitized by *T. sinensis*, predicts that, starting from non-zero densities of both species, the subsequent dynamics will continue to have non-zero densities at all later years, with upper bounds determined by the availability of buds (for *D. kuriphilus*) and of galls (for *T. sinensis*; see sec. 5.3.1 for the mathematical proof). This property alone, however, does not guarantee the survival of either species. If, at some point in time, the modeled egg density of a species drops to sufficiently low values, then the model is predicting a local extinction of that species. An order-of-magnitude estimate of the threshold density that signals extinction may be obtained as follows: a full-grown chestnut tree in spring produces about 10^4 buds; typical production orchards have a density of 100 – 200 trees per hectare, while coppices may have up to 1000 stems per hectare, but with less buds per stem than in individual trees (Bounous, 2014). Thus we have $\beta_{max} \approx 2 \cdot 10^6$ buds ha⁻¹, and, allowing for uncertainties

in the above figures, it follows that V_{max} ranges between $10^7 - 10^8$ eggs ha^{-1} . Therefore, non-dimensional densities v_n, q_n below $10^{-7} - 10^{-8}$ correspond to less than one insect per hectare. For an isolated, hectare-wide orchard, this would be the extinction threshold. For a chestnut woodland spanning several square kilometers the threshold would be proportionally lower.

The map (23) depends on three parameters: η, E_T, k . The last two, in turn, depend on other parameters, namely γ, N_T, η, N_D and μ (see Tables 1 and 2). We shall discuss the dynamics of the map as a function of the overwintering survival fractions η and γ (owing to the uncertainty of their value) and fix the other parameters to the following values: $N_D = 150$ (eggs per *D. kuriphilus* adult), $N_T = 70$ (eggs per *T. sinensis* female adult), $\mu = 10$ (ratio of lengths of the season and individual life span for *D. kuriphilus*). Uncertainties in the value of μ do not produce large changes: going from $\mu = 3$ to $\mu = 20$ gives about 15% difference in the value of the constant k_- in (13). In Figures 2 to 5 we use $k = k_-$, because this choice gives a better approximation at low densities. Note that using $k = k_+$, is equivalent to using a larger value of E_D with $k = k_-$. In order to avoid inaccuracies due to numerical cancellation errors, all calculations for producing the figures have been carried out with 200 decimal significant digits, using an arbitrary precision numerical library Johansson et al. (2013). A more general and technical analysis of the map is given in Appendix 5.3.

Depending on the values of η and γ there are 4 possible dynamical outcomes qualitatively distinct: extinction of both species, extinction of the parasitoid, steady coexistence, and predator-prey cycles. The first 3 occur for unrealistically low values of these parameters. If η is as low as to make $k < 1$ in (23), then the egg density of *D. kuriphilus* asymptotically goes to zero. As the gall wasp goes extinct, so does *T. sinensis*, for lack of galls where to lay eggs. This region of the parameter space is represented by the white vertical strip in Figure 2 (top panel). If η is such that $k > 1$ and γ is sufficiently low, then only *T. sinensis* becomes extinct, and *D. kuriphilus* reaches the non-zero fixed point of Skellam's map (12). This is the gray region in Figure 2 (top panel). The exact threshold value of γ_{tr} cannot be expressed in simple terms, but a good approximation (the white dashed line in Figure 2, top panel) is

$$\gamma_{tr} \approx \frac{1}{N_T(1 - e^{-\eta})}. \quad (24)$$

The dark blue region above the threshold in Figure 2 (top panel) corresponds to the survival fractions at which both species survive and reach a stable fixed point. The shape of this region shows that, according to the model, a steady coexistence of both species may only occur if the overwintering survival fraction of at least one of the two species is unrealistically low.

When it exists, we find a unique coexistence fixed point. It can be visualized as the intersection between the set of points (v_n, q_n) such that $q_{n+1} = q_n$ (the green lines in the right panel of Figures 3, 4, 5) and the set of points (v_n, q_{n+1}) such that $v_{n+1} = v_n$ (the red lines in the right panel of Figures 3, 4, 5). We shall call these sets, respectively, q -nullcline and v -nullcline, and they intersect, at

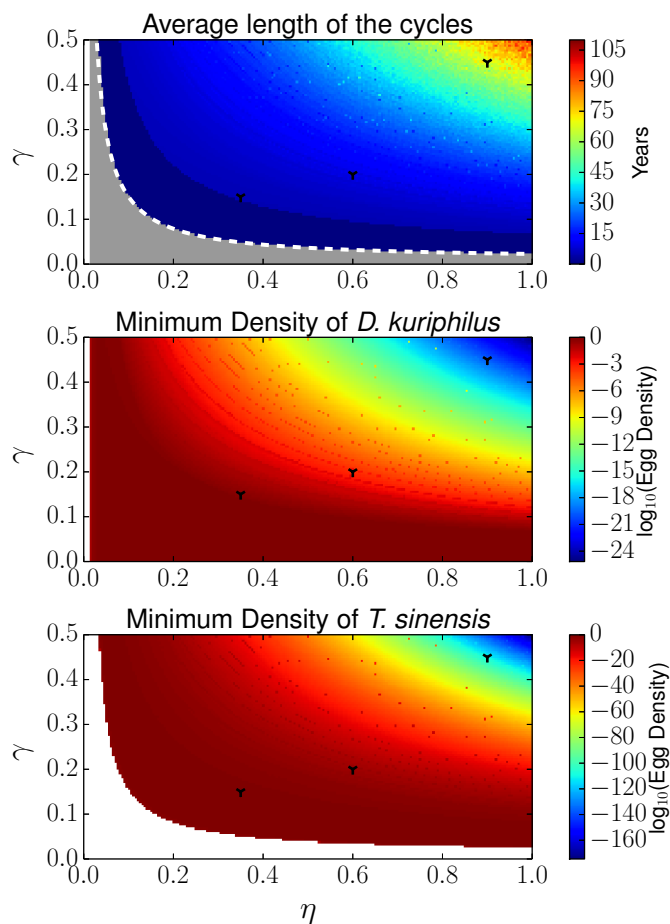


Figure 2: As a function of the overwintering survival fractions η and γ , top panel: average length of the predator–prey cycles; zero means that the coexistence fixed point is stable; the gray area that *T. sinensis* asymptotically becomes extinct; the white area that both species asymptotically become extinct; the white dashed line is the graph of (24). Middle panel: \log_{10} of the minimum density of *D. kuriphilus* eggs; the white region corresponds to asymptotic extinction. Lower panel: \log_{10} of the minimum density of *T. sinensis* eggs; the white region corresponds to asymptotic extinction. For each pair (η, γ) the statistics are computed over 3000 iterations of the map, after a 2000 iterations transient. The black markers show the parameters of Figures (3), (4), (5). Note that γ , the survival fraction of *T. sinensis*, also includes the sex ratio, and therefore may not be greater than 0.5.

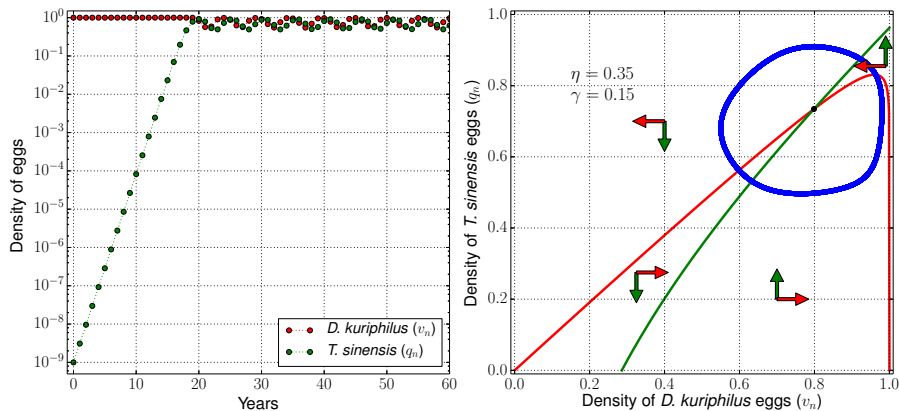


Figure 3: Left panel: time evolution of *D. kuriphilus* (red dots) and *T. sinensis* (green dots) egg density when the fraction of (female) larvae surviving the overwintering is, respectively $\eta = 0.35$ and $\gamma = 0.15$; see the text for the other parameters. Right panel: the red and the green curves are, respectively, the v -nullcline and the q -nullcline, which partition the plane in four regions; their intersection, marked by the black dot, is the unstable coexistence fixed point; the blue loops shows the states that the system occupies for asymptotically large times; the red horizontal arrows and the vertical green arrows show, for each of the four regions, whether the densities of the next state will be larger or smaller than those of a state in that region.

most, at a single point (see Appendix 5.3.2 for details). If the overwintering survival fractions η and γ in Figure 2 (top panel) lie beyond the dark blue region of steady coexistence, a coexistence fixed point still exists, but is unstable, therefore the insect egg densities fluctuate from year to year. When q_n is above the q -nullcline, then $q_{n+1} < q_n$, and if q_n is below, then $q_{n+1} > q_n$. Analogously, when v_n is above (below) the v -nullcline, then v_{n+1} is smaller (larger) than v_n . These drop or raise tendencies are depicted in the left panel of Figure 3, by the green vertical arrows for q_n , and by the red horizontal arrows for v_n . The arrows in the right panel of Figure 3 suggest that the sequence of states in a q_n vs v_n diagram rotates anticlockwise around the unstable fixed point, corresponding to cyclical increases and decreases of both species, in which maxima and minima of *T. sinensis* follow the maxima and minima of *D. kuriphilus*, yielding the kind of fluctuations that are ubiquitous in predator-prey dynamics (e.g. May and McLean, 2007, ch. 5). For generic values of η and γ these fluctuations are not periodic, nor asymptotically approach a periodic oscillation. However the cycles are characterized by a fairly well-defined time scale.

Figure 3 (left panel) shows 60 years of dynamics that one obtains by adopting for the overwintering survival fractions the very low values $\eta = 0.35$ and $\gamma = 0.15$, located just beyond the steady coexistence region. The initial state is designed to simulate the release of a tiny amount of *T. sinensis* in a large chestnut forest infested by *D. kuriphilus*. Thus we take $v_n = 1$ and $q_n = 10^{-9}$. During the first two decades the population of *T. sinensis* grows steadily

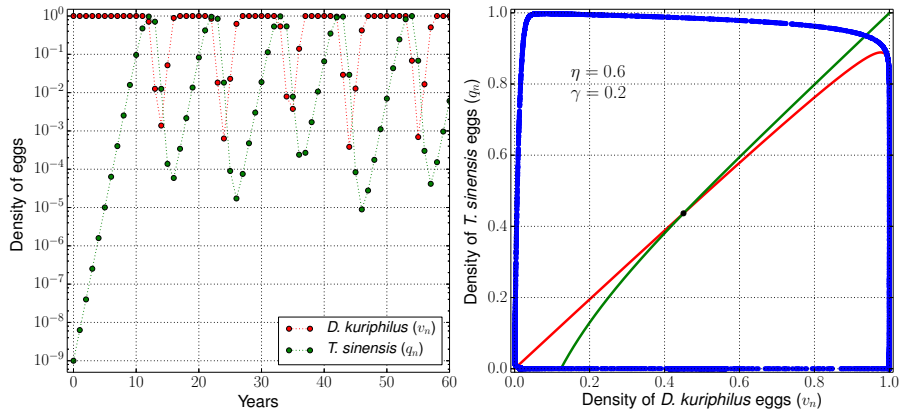


Figure 4: As Figure 3, but with $\eta = 0.6$ and $\gamma = 0.2$. These parameters might be representative of a situation in which *T. sinensis* suffers from hyperparasitism, as it is hypothesized for Japan.

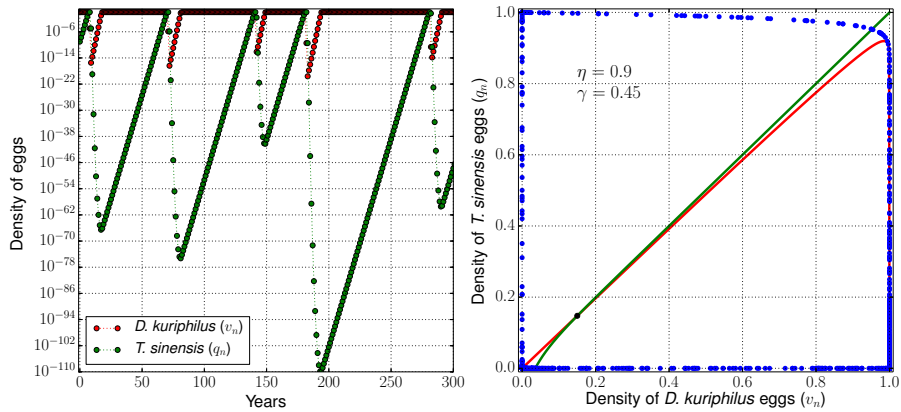


Figure 5: As Figure 3, but with $\eta = 0.9$ and $\gamma = 0.45$. These are parameters that we consider to be realistic for Europe. Note the extreme excursion of densities and the logarithmic density axis of the left panel.

from the very low initial density, while the population of *D. kuriphilus* remains essentially unaffected by the presence of the parasitoid. When q_n approaches 1, then v_n begins to decline. From then on, the densities of the two species oscillate in cycles that are about 5 years long. Omitting the initial transient, and plotting q_n vs v_n one finds that the succession of states describes the blue loop depicted in Figure 3 (right panel). With these low survival fractions the loop winds relatively close to the unstable fixed point (the black dot at the intersection of the nullclines). Note that with these parameters the biological control is not achieved in a satisfactory way: the egg density of *D. kuriphilus* never drops below 50% of its initial value.

In Figure 4 we show the dynamics when the overwintering survival fractions are increased to $\eta = 0.6$ and $\gamma = 0.2$. Albeit still low, these values might represent the case of Japan, where, according to Murakami and Gyoutoku (1991), a large amount of non-specialist parasitoid and hyperparasitoids species, assumed to be always present in the environment at a roughly constant concentration, cause a high overwintering mortality both in *D. kuriphilus*, and, even more, in *T. sinensis*. The left panel of Figure 4 shows that the transient growth of *T. sinensis* is shortened to about a decade, after which it starts to dent the population of *D. kuriphilus*. The cycles after the transient have a length of 10–11 years, which is a time scale that roughly matches the observations in Japan (Moriya, personal communication). In the model, the egg concentration of *D. kuriphilus* remains almost constant, and very close to 1, for 6–7 years, while the density of *T. sinensis* grows. Then, in the turn of 1–2 years *T. sinensis* peaks and causes a sudden drop in the concentration of *D. kuriphilus*, and consequently, also the population of *T. sinensis* drops in the following years. The recovery of *D. kuriphilus* occurs in 1–2 years, starting from minimum densities that may be smaller than 10^{-3} . The population of *T. sinensis* continues to drop until the recovery of *D. kuriphilus* is almost complete, then it starts to increase. By this time the density of *T. sinensis* may have reached densities almost as low as 10^{-5} . The decline and the subsequent recovery of *T. sinensis* span almost all the length of the cycle. High densities of *T. sinensis* occur only for 2–3 years in each cycle. The right panel of Figure 4 shows the succession of states (in blue, the initial transient was omitted) looping anticlockwise around the unstable fixed point (the black dot). In this case the loop is pushed much further away from the fixed point than in Figure 3, and the densities v_n , q_n almost always assume either very low values or values close to 1. Even in this case a satisfactory biological control is not achieved.

This kind of dynamics, in which *D. kuriphilus* remains most of the times at densities close to 1, interrupted by brief bursts in the population of *T. sinensis*, rather than performing mild oscillations at intermediate values, occurs every time that the overwintering survival fractions are significantly removed from the stability region of the fixed point. For example, if the overwintering survival fractions are increased to values that we consider realistic for Europe, such as $\eta = 0.9$ and $\gamma = 0.45$, we observe the same stasis and burst dynamics as in the previous case, but with much longer cycles, that may last several decades (Figure 5). However, the really remarkable feature of this case is the extreme

depth of the drops in the population density of both species. The left panel in Figure 5 shows that when the egg density of *T. sinensis* becomes close to 1, then the egg density of *D. kuriphilus*, in a single season, drops to values that may be smaller than 10^{-20} . The subsequent recovery of *D. kuriphilus* is not short, but requires several years, during which the population of *T. sinensis*, for lack of deposition sites, decreases to absurdly low values. As we argued at the beginning of this section, cycles that reach minima this low are a mathematical fiction. In reality, the model is stating that *T. sinensis*, after the initial transient, wipes out the local population of *D. kuriphilus*, and then becomes extinct itself. We would like to stress that this is really a fifth dynamical regime, and it should not be confused with the extinction that takes places at the opposite end of the parameter space, when the overwintering survival fractions are very close to zero.

The three panels of Figure 2 show, from top to bottom, the average length of the cycles, and the minimum density attained during a cycle for *D. kuriphilus* (middle panel) and *T. sinensis* (lower panel) as a function of η and γ . Note that all reasonably high values of the survival fractions yield long cycle lengths and extremely low densities at minimum, signaling the extinction of both species. However, this does not necessarily means that the map is forecasting a successful biological control. Because the minima of *T. sinensis* are generally much lower than those of *D. kuriphilus*, there is the possibility that *T. sinensis* reaches extinction-level densities before *D. kuriphilus*, which would then remain completely unchecked.

Finally, we mention that, for selected values of η and γ , the map (23) appears to be characterized by periodic cycles with amplitude and length smaller than those found at different, but very close, values of the parameters (these are the scattered dots of color slightly different than the surroundings visible in Figure 2). These *regularity windows* are commonplace in discrete-time dynamical systems such as the map (23) and are unlikely to persist if subject to the random perturbations that are always present in a natural environment, but are absent in this simple model. Thus their presence does not change the overall qualitative description of the dynamics given above.

3.2. Space-dependent dynamics of *D. kuriphilus*

Before discussing the complete model (22) it is appropriate to analyze the dynamics of *D. kuriphilus* alone, as it invades an idealized forest. We shall consider a 1-dimensional spatial domain, that could be thought of as a very long strip of trees whose width is negligible with respect to its length.

If *D. kuriphilus* is released at one end of the strip, in the absence of *T. sinensis*, the equations (7), and their non-dimensional counterpart (8), describe the propagation of the population of the pest as it invades the domain. This is a traveling front joining the region in which the forest is fully infested by the pest to the region in which the pest is still absent, as illustrated in Figure 6A. Note that, owing to the large number of eggs that can be laid by a single individual, a relatively small density of adults is sufficient to saturate all of the available buds. Therefore, at the end of the season, the egg density front is offset with

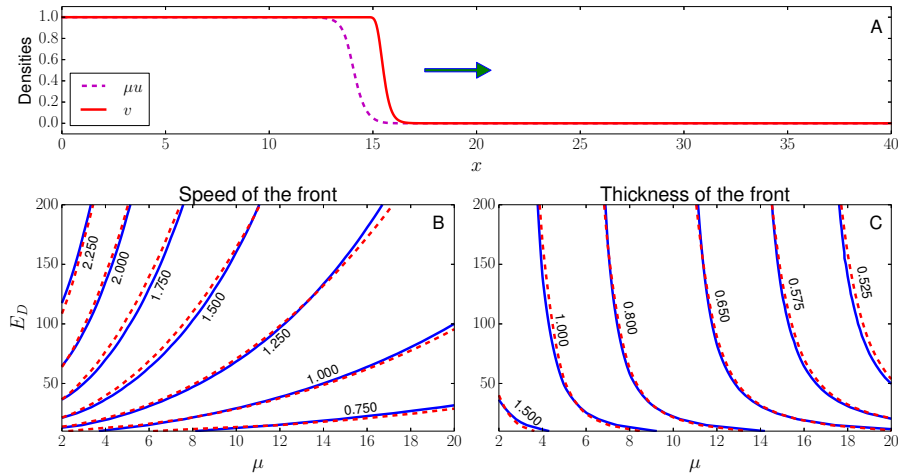


Figure 6: A) Density of eggs (continuous line) and of adults (dashed line) of *D. kuriphilus* at the end of the 10th season in a numerical solution of equations (8) with $\mu = 10$ and $E_D = 135$, where the pest is initially introduced at the left end of the one-dimensional domain. For clarity the density of adults is multiplied by μ . The arrow shows the direction of propagation of the front. B) Contour lines of the speed of the front as a function of the parameters μ and E_D . The solid lines are the numerical results, and the dashed lines are the fit $(1.95(E_D - 8)^{1/5})/(\mu + 2.75)^{1/2}$. C) Contour lines of the thickness of the egg density front as a function of the parameters μ and E_D . The solid lines are the numerical results, and the dashed lines are the fit $((2.26E_D + 7)/E_D)/(\mu + 0.1E_D^{1/2})^{1/2}$. All quantities in these figure use the non-dimensional units of Table 2.

respect to the density front of the adult population. Numerical simulations (we used centered, second-order, finite-differences discretization for the diffusion term and Heun's method for timestepping) show a strong analogy with the propagation of a burning front, and the solutions are reminiscent of those of the well-known Kolmogorov-Fisher equation, which is the prototypical example for this kind of phenomena (see e.g. Murray, 2007, § 13.2). For the K-F equation a simple argument based on dimensional analysis shows that the speed and thickness of the front are directly proportional to the square root of the diffusion coefficient. The thickness is also directly proportional to the characteristic time of the chemical reactions, but the speed is inversely proportional to it.

Equations (7) are more complicated. The change of variables that brings (7) into (8) also suggests a proportionality of speed and thickness of the gall wasp front to the square root of the diffusivity. However, there are three distinct time scales that characterize the reaction-like terms of equations (7): the season length T_D , the individual life span a , and the reciprocal of the egg deposition rate, a/N_D . Thus, in the non-dimensional equations (8) there remain two independent parameters, namely E_D and μ . Figures 6B and 6C show the dependence of speed and thickness of the front on E_D and μ in a wide range of values. These data (represented by the solid lines) use the non-dimensional units of Table 2. In particular, the unit of length is $\sqrt{D_D T_D}$ and the unit of

speed is $\sqrt{D_D/T_D}$. The speed of the front is evaluated as the speed of the point where the non-dimensional egg density v is equal to 1/2. The thickness of the front is estimated as $(\partial v/\partial x)^{-1}$, where the derivative is evaluated at the same point. Both quantities are computed from the results of numerical solutions of the equations (8) subject to the conditions (9) and (10). The data may be fitted reasonably well with simple analytic expressions (dashed lines, see the figure captions for their expression in terms of E_D and μ). In terms of dimensional variables, and of the parameters of Table 1, the fits for the speed S and the thickness Δ of the front read

$$S = 1.95 (\eta N_D - 8)^{1/5} \sqrt{\frac{D_D}{T_D \left(\frac{T_D}{a} + 2.75\right)}}, \quad (25)$$

$$\Delta = \left(\frac{2.26\eta N_D + 7}{\eta N_D}\right) \sqrt{\frac{T_D D_D}{\frac{T_D}{a} + 0.1\sqrt{\eta N_D}}}. \quad (26)$$

These expressions are not formally deduced from the equations (we postpone this issue to a future work), and thus should be considered to be reliable only within the parameter range of Figures 6B and 6C. Nevertheless, they are fully satisfactory for the problem of determining the magnitude of the diffusion coefficient D_D on the basis of the observed propagation speed of the pest. Taking into account that each year the gall wasp is active and mobile only during the interval of time T_D , the speed of the front can also be expressed as $S = L/T_D$, where L is the length traveled in one year by the infestation (as reported by EFSA, 2010).

Taking $T_D = 40$ d, $a = 4$ d, $\eta = 0.9$, $N_D = 150$, from (25) we find

$$D_D \approx \frac{L^2}{83} \quad (27)$$

where the denominator is expressed in days. Using this in (26) we can link the thickness of the front to the length it travels in a season, finding

$$\Delta \approx \frac{L}{2.1}. \quad (28)$$

For example, with $L = 8$ km, we have a thickness of the front $\Delta \approx 3.8$ km, and a diffusion coefficient $D_D \approx 0.77$ km²d⁻¹. With a numerical value for the diffusion coefficient we can explicitly convert our non-dimensional lengths in kilometers, finding that, in this example, one unit of length is $\sqrt{D_D T_D} \approx 5.5$ km.

Assuming that the trajectories of individual insects approximate a Brownian motion, Einstein's formula (see, e.g., Gardiner, 2004, §1.2) suggests that the typical displacement l of an adult after t days would be $l = \sqrt{2nD_D t}$, where n is the dimensionality of the domain. Thus, in our idealized 1-dimensional strip of trees the displacement over the entire adult life span (4 days) would be $l \approx 2.5$ km, and in a 2-dimensional domain, such as a real wood, it would be $l \approx 3.5$ km.

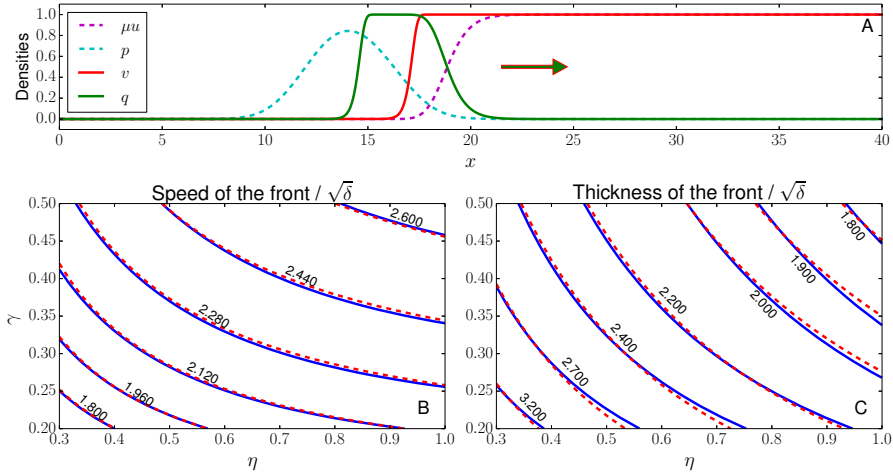


Figure 7: A) Density of eggs (red continuous line) and of adults (magenta dashed line) of *D. kuriphilus* density of eggs (green continuous line) and adults (cyan dashed line) at the end of the 7th season in a numerical solution of equations (22) with $\mu = 10$, $E_D = 135$, $E_T = 31.5$, $\gamma = 0.45$, $\eta = 0.9$, $\delta = 1$, $\tau = 1/\eta$, where the pest is initially homogeneously distributed throughout the one-dimensional domain, and the parasitoid is present only at its left end. For clarity the density of adults of *D. kuriphilus* is multiplied by μ . The arrow shows the direction of propagation of the front. B) Contour lines of the speed of the front as a function of the overwintering survival fractions η and γ . The solid lines are the numerical results, and the dashed lines are the fit $(\eta/(0.301\eta + 0.021))(\gamma - 0.05/(\eta + 0.12))^{1/5}$. C) Contour lines of the thickness of the egg density front as a function of the overwintering survival fractions η and γ . The solid lines are the numerical results, and the dashed lines are the fit $((0.88\eta + 1.55)/(0.6 + \eta))(\gamma - (1 - 0.6\eta)/(17\eta))^{-1/5}$. For values of δ different from 1, an excellent fit is obtained by multiplying these expressions by $\sqrt{\delta}$. All quantities in these figure use the non-dimensional units of Table 2.

3.3. Space-dependent dynamics of the host–parasitoid system

If we start from an initial condition in which the idealized 1–dimensional forest is fully infested by the pest, and the parasitoid is introduced at its left end, then, in the course of years, the parasitoid population will propagate rightward, as depicted in Figure 7A. As the parasitoid propagates rightward, it causes a severe drop in the population density of the pest, which develops a left–facing region of high gradient, connecting the part of the forest which has not yet been reached by the parasitoid, and thus is still fully infested, to the part already swept by the parasitoid, where the pest density has been severely reduced. The reduction in the pest density is mirrored by a corresponding reduction of the parasitoid density, which faces a drastic scarcity of its host in the region of the forest that has already been swept. Therefore, the parasitoid population propagates into an infested forest as a moving peak, rather than as a moving kink.

The results of the numerical simulations show that the speed of propagation of the parasitoid, and the thickness of the right–facing gradient region of its egg density, are proportional to the square root of the diffusivity ratio $\sqrt{\delta}$ (see Table 2), with excellent approximation, at least in the interval $\delta \in [0.1, 10]$. We have also computed the dependence of speed and thickness on the overwintering survival fractions η and γ . The results are reported in Figures 7B and 7C. These results may be fitted by simple expressions, which, in terms of the parameters of Table 1, read:

$$S_T = \frac{\eta}{0.301\eta + 0.021} \left(\gamma - \frac{0.05}{\eta + 0.12} \right)^{1/5} \sqrt{\frac{D_T}{D_D}}, \quad (29)$$

$$\Delta_T = \frac{0.88\eta + 1.55}{0.6 + \eta} \left(\gamma - \frac{1. - 0.6\eta}{17\eta} \right)^{-1/5} \sqrt{\frac{D_T}{D_D}} \quad (30)$$

These expressions are valid when the other parameters are $\mu = 10$, $E_D = 135$, $E_T = 31.5$, $\tau = 1/\eta$, which should represent fairly well the relevant physiological parameters of both the pest and of the parasitoid, as discussed in §2.4.

The density to which both the pest and the parasitoid drop on the left–hand side of the right–moving peak, depends on the value of the overwintering survival fractions η and γ , roughly in the same way as shown in Figure 2 for the spatially homogeneous case discussed in §3.1. At low and intermediate survival rates (such as those of Figures 3 and 4) the density drop spans at most a few orders of magnitude, and it is thus insufficient to justify hopes of eradication of the pest.

At higher survival rates the severity of the density drop is as large as to amply justify claims of local extinction: as the parasitoid sweeps the forest, virtually no host will be left unparasitized. Unfortunately, this effect alone does not guarantee a successful biological control. In fact, our model shows cases in which the pest is able to recolonize the empty forest left back by the passage of the parasitoid.

Figure 8 illustrates this phenomenon. In order to demonstrate that the model really allows for cases of recolonization, rather than failures of the parasitoid

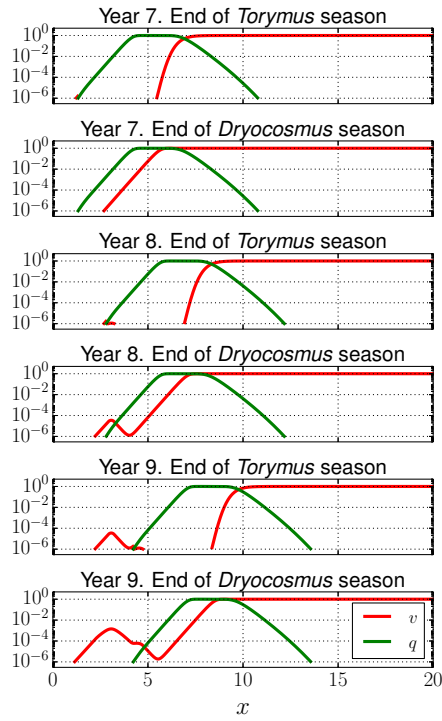


Figure 8: A time sequence showing the beginning of the recolonization of the forest by the pest after the passage of the parasitoid. The red line is the density of eggs or unparasitized larvae of the pest *D. kuriphilus*; the green line is the density of eggs or larvae of the parasitoid *T. sinensis*. Note the logarithmic scale. The ratio of the diffusivities (see Table 2) is $\delta = 0.3$, the other parameters are the same as in Figure 7A.

to attain a complete local eradication of the pest, in the run that produced Figure 8, at the end of the *Torymus* and of the *Dryocosmus* seasons, the egg density of both species was set to zero anywhere it was found to be below a threshold of local extinction equal to 10^{-6} non-dimensional units. The rationale of identifying areas of very low density in the model as areas where no individual insects are likely to be present was discussed at the beginning of §3.1. In this run the initial conditions correspond to a release of a small amount of parasitoid in a region spanning 1 non-dimensional units on the left end of the idealized 1-dimensional forest saturated by the pest. In a few years the population of the parasitoid grows and spreads rightward into the forest, locally wiping out the pest, and leaving a region devoid of both host and parasitoid behind its passage.

The time sequence of Figure 8 begins 7 years after the release of the parasitoid. At the end of the *Torymus* season, little or no *Dryocosmus* larvae remain unparasitized in correspondence of the peak density of the parasitoid (Figure 8, panel “Year 7 - End of *Torymus* season”). Then the surviving larvae of *Dryocosmus* emerge, and diffuse in the forest, looking for deposition sites. By the end of the season, much of the ground lost to *Torymus* is recovered by *Dryocosmus*, that arrives to lay some eggs even in the region on the left of the *Torymus* peak, where the presence of the parasitoid is dwindling because of the scarcity of the host. Thus, at the end of year 7, on the left of the *Torymus* peak, both host and parasitoid are present, and, moving leftward, their density declines at a similar rate (Figure 8, panel “Year 7 - End of *Dryocosmus* season”). The next year *Torymus* once again wipes out all *Dryocosmus* larvae in the region where its density is highest, and continues its march rightward. However, on the left end of the *Torymus* peak, the density of the parasitoid is so low that it is unable to control the pest. Therefore, the very small amount of *Dryocosmus* larvae originating from the eggs that were laid on the extreme left of the *Torymus* density peak, are left virtually unaffected by the presence of the parasitoid (Figure 8, panel “Year 8 - End of *Torymus* season”). Thus, they are able to develop into *Dryocosmus* adults, that find, on their left, a forest devoid of the parasitoid and ready to be recolonized (Figure 8, panel “Year 8 - End of *Dryocosmus* season”). In the next year the recolonized patch widens to the left, and the density of the pest increases (Figure 8, “Year 9” panels). In the following years (not pictured in Figure 8), when the pest density has recovered to sufficiently high density values, a second peak of the parasitoid population splits from the first, sweeping leftward the recolonized forest. Subsequently, the pest passes back through this second peak, just as it did with the first. With the choice of parameters of the run in Figure 8, the long term dynamics is a never ending alternation of local extinctions and recolonizations.

The inability of the parasitoid to control the pest at low densities of both species derives from the very low probability of finding egg deposition sites when both host and parasitoid are rare. This is a general characteristic of predator-prey systems and the ultimate source of their cyclic behavior. In the case of the present model, for spatially homogeneous solutions, a mathematical analysis of this effect is given in §5.3.3 (equation (42) and the following discussion). For solutions that have a dependence on space, local population flows caused by

diffusion become important, and this means that regions where the pest had been eradicated and thus the parasitoid has dropped to densities at which it is unable to exert an effective control, may come again within reach of the diffusing pest population, as we have illustrated discussing the Figure 8.

In order to understand under which conditions the pest is able to cross the parasitoid peaks and recolonize the forest, we have examined a large sample of numerical solutions of the model equations, with different parameters. The general pattern that emerges is the following: if the speed of propagation of *Torymus* peaks (as given by eq. (29)) is appreciably larger than that of *Dryocosmus* fronts (eq. (25)), then the pest will not be able to recolonize the forest. Conversely, if the speed of *Dryocosmus* fronts is sufficiently larger than that of *Torymus* peaks, then recolonization occurs. The precise boundary between the two regimes is determined by the value of the threshold of local extinction.

The dynamics of traveling fronts of *Dryocosmus* and of sweeping peaks of *Torymus* is present also when the spatial domain is two-dimensional. In this case, peaks and fronts may be verbally described as waves propagating through the forest, as illustrated in the time sequence of Figure 9. The *Torymus* is initially released close to the lower-right corner of a square forest (the size of 20×20 non-dimensional units corresponds in this numerical solution to a physical size of approximately 110×110 km). It spreads radially, leaving a roughly circular area of the forest free of both the pest and the parasitoid, which is quickly recolonized by the pest. The parasitoid population then splits in two parts: most of it continues to propagate through the forest in an expanding arched wave, and a small part returns close to the release site, hunting the pest that has recolonized the release area, giving rise to a second expanding arching wave (left column of Figure 9). On longer time scales, because of the interaction with the forest boundaries, these waves assume irregular shapes and form a large variety of patterns (right column of Figure 9). The basic recolonization mechanism, however, remains the same, and repeats endlessly.

This means that the time scales of appearance and disappearance through the years of both pest and parasitoid at any fixed place in the forest are determined by the speed of propagation of the waves, and by the size and shape of the forest itself. This is illustrated in Figure 10, showing the end-of-year egg density of *Dryocosmus* and *Torymus* at the *Torymus* release site, in the numerical solution of Figure 9. In this case we have tuned the diffusivity ratio (namely, we used $\delta = 0.2$) explicitly to obtain cycles of pest and parasitoid on a decadal time scale (roughly the same time scale as observed in Japan). Note that, with these parameters, and neglecting the extinction threshold, homogeneous solutions would give the cycles shown in Figure 5, that have a much longer time scale. The space-dependent solutions, instead, have the same time scale of the homogeneous solutions of Figure 4, but with much higher overwintering survival fractions.

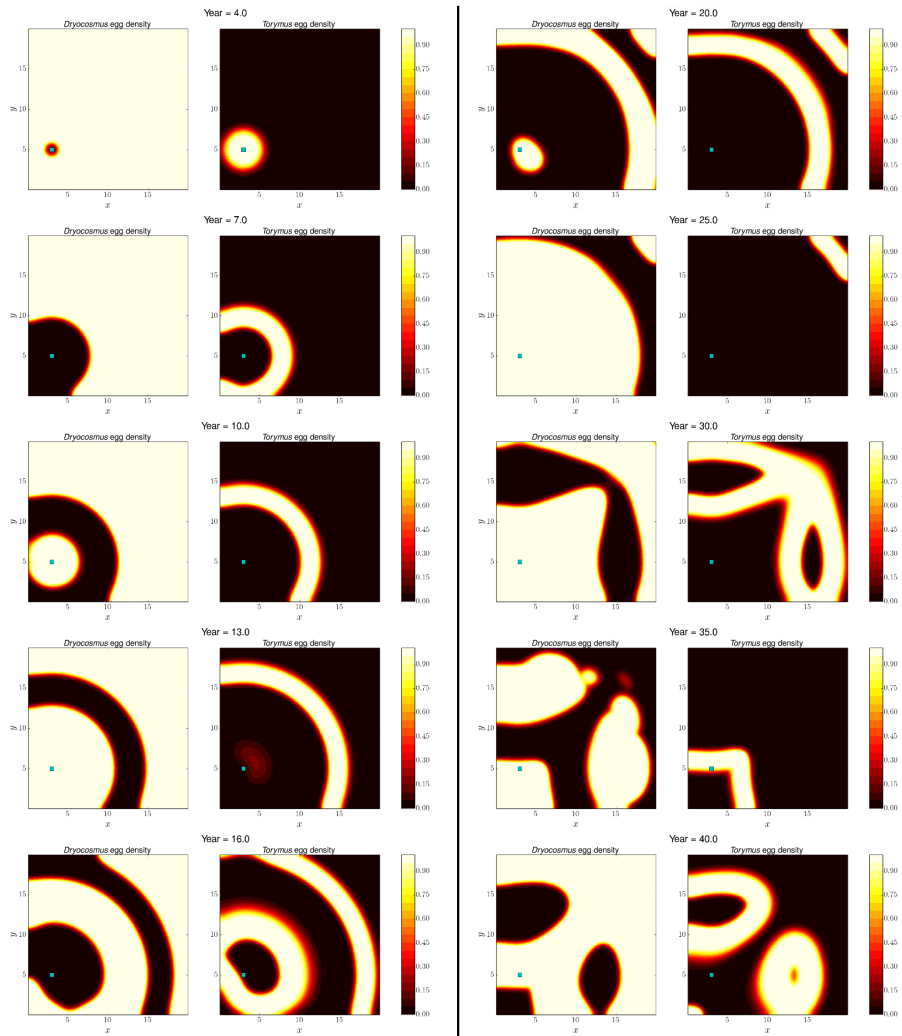


Figure 9: Time sequence of *D. kuriphilus* (left panels) and *T. sinensis* (right panels) egg densities in a numerical solution of the model equations with $\delta = 0.2$ and the other parameters as in Figure 8. The left column shows the earlier years after the release of a small amount of *T. sinensis* in a small patch of a square forest saturated by *D. kuriphilus*. The right column shows the dynamics on a longer time scale. The marker visible close to the lower left corner of all the panels is the release site of *T. sinensis*, and the place where the egg densities shown in Figure 10 are measured.

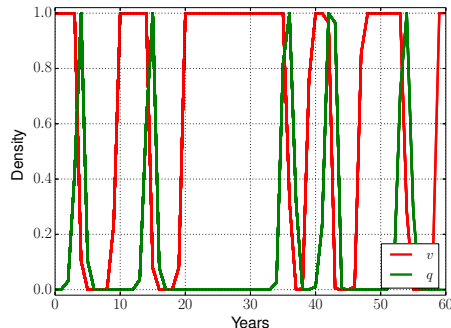


Figure 10: Densities of *D. kuriphilus* (v) and *T. sinensis* (q) eggs, at the end of each year, measured at the *T. sinensis* release site (shown in Figure 9) in the numerical solution of the model equations shown in Figure 9.

4. Discussion and conclusions

In this paper we have developed a spatially explicit model that describes the invasion of a chestnut forest by the gall wasp *Dryocosmus kuriphilus*, which acts as pest of the chestnut outside its native China, as well as the effect of the parasitoid *Torymus sinensis*, which is modeled as host-specific of the gall wasp and perfectly synchronized to its life cycle. In the special case of a spatially homogeneous distribution of both pest and parasitoid, the model can be reduced to an iterated map. Otherwise it is a set of piecewise time-continuous reaction-diffusion partial differential equations which describe the spread and the competition for egg deposition sites of the adults of both species.

The primary aim of the model is that of elucidating the possibilities of obtaining a biological control of the gall wasp, and understanding possible causes of failure in obtaining control. In this respect the crucial parameters are the overwintering survival fractions (the fraction of laid eggs that successfully emerge the next year) and the diffusion coefficients of the two species.

If the overwintering survival fractions are sufficiently far from 100%, then both the spatially explicit model and its spatially-independent counterpart show persistent oscillations in the density of both species, reminiscent of the classic predator-prey models, having an amplitude too small to be consistent with local extinction. This is in agreement with the hypothesis of Murakami and Gyoutoku (1991), that attributes the failure of achieving biological control in Japan to the presence of non-specialist parasitoid and hyperparasitoids species, which would cause a high overwintering mortality.

Our own observations strongly suggest that, in an European setting, the overwintering survival fractions are, at least, 90%. In that case, in a spatially homogeneous situation, the model exhibits drops of more than 15 orders of magnitude in the density of the pest, followed by even larger drops in the density of the parasitoid. In practical terms, drops of this magnitude can only be interpreted as signaling the local extinction of the insect. Thus, in a spatially

homogeneous situation, and with parameters that we consider appropriate for the European setting, the model predicts that the parasitoid would quickly eradicate the pest.

However, ever since the seminal experiments of Huffaker (1958) on mites, it is known that spatial inhomogeneities may delay or altogether avoid phenomena of local extinction in predator–prey systems. In particular, spatially explicit versions of the Nicholson–Bailey host–parasitoid model show that the dispersal of the individuals spontaneously produces the formation of complicated, time-varying, but persistent patterns. In these cases, forcing a spatially–homogeneous environment (e.g. by reducing the size of the domain below the intrinsic scale of the patterns) often results in a rapid local extinction of both the host and the parasitoid (Hassel et al., 1991).

With our model we find a similar outcome. If the speed of propagation of the host population is faster than that of the parasitoid population (those speeds are strongly dependent on the diffusion coefficients of the two species) and the size of the domain is sufficiently large, then the spatially explicit model never settles into a spatially–homogeneous solution leading to extinction. Instead, the gall wasp recolonizes the areas left empty after the passage of the parasitoid, in a never ending sequence of crossing waves of population density, of which Figure 9 shows an example. We should note that the imperfect biological control achieved in Japan should probably be explained in this way, because the attack rate of indigenous parasitoids was later found to be no larger than 2% (EFSA, 2010), thus making unlikely the hypothesis of low overwintering survival rates.

On the other hand, when the population of the parasitoid propagates sufficiently faster than that of the pest, then a single density wave of the parasitoid sweeps the forest, killing the host, and leaving neither species behind it. In this case the end result of the spatially explicit and of the spatially homogeneous models is the same, and they both suggest a complete eradication of the pest.

Quite remarkably, the literature does not appear to contain any quantitative observation of the speed of propagation of *Torymus sinensis* when it is released in a forest fully invaded by *Dryocosmus kuriphilus*. In the United States, after the release there has been a 30 years lapse with no follow-up observations (Cooper and Rieske, 2007). In Japan the published data refer to insect densities at the release site (Moriya et al., 1989; Murakami et al., 2001; Moriya et al., 2003) but give no information on the spatial patterns of the insect population densities and their changes in time. In Europe the releases of *T. sinensis* have begun only a few years ago, and we are not aware of surveys assessing their spatial distribution in the following years. On the basis of qualitative personal observations the authors suspect that *T. sinensis* actually spreads at a much lower rate than *D. kuriphilus*. If this were confirmed by quantitative measurements, then, according to the model, we should expect that the release of *T. sinensis* at a single location within a large forest area would simply trigger a train of density waves of both the pest and the parasitoid, that would travel into the forest producing, at any fixed site, an alternating presence and absence of the insects on decadal time scales. A satisfactory control would then only be achieved by follow-up releases of the parasitoid, continuing for many years, at

carefully chosen sites, in order to suppress any returning wave of *D. kuriphilus* that could recolonize the forest left empty by the previous sweep of *T. sinensis*. This strategy, obviously, calls for a campaign of accurate observations tracking the spatial distribution of both species in the course of several years.

An important part of the model is the choice of describing the dispersion of the individuals with diffusion operators. This is correct if the overall motion of the individuals may be characterized by random flights, and the length of the flights has a distribution with Gaussian or shorter tails. Recently, it emerged that some animals appear to move by performing so-called Lévy walks, that is, random trajectories approximated by sequences of straight segments, where the probability distribution of the lengths of each segment has long, algebraic tails, and the variance of the distribution diverges. This movement strategy should be advantageous when searching for randomly scattered resources, in particular if they have a fractal distribution (Viswanathan et al., 2008). If *D. kuriphilus* or *T. sinensis* adopted this strategy, then the model would have to be corrected with the use of fractional diffusion operators, rather than ordinary ones. However, under the Lévy walk hypothesis, a substantial fraction of the length traveled by each insect during its lifetime would be traveled with just a few straight legs. While straight flight is very likely to occur on scales of the order of a meter, where visual and olfactory cues may reliably direct the animal straight to its target, lacking published evidence, it seems far-fetched to assume that the individuals of *D. kuriphilus* or *T. sinensis* are consistently able to travel several hundred of meters, or kilometers, along a straight line, within the canopy of a forest, maintaining a precise bearing. We find further support in our belief that *D. kuriphilus* and *T. sinensis* do not perform Lévy walks from the mathematical result that equations of the sort discussed in §3.2, but with fractional diffusion, would generate traveling fronts that exponentially accelerate, rather than maintain a constant speed (del-Castillo-Negrete et al., 2003). We are not aware of any report of acceleration of a gall wasp invasion front.

The fact that Lévy walks are unlikely to be the dispersion mechanism of the pest and of the parasitoid, does not mean that other dispersion processes, in addition to ordinary diffusion, should be ruled out. The gall wasp spreading model of EFSA (EFSA, 2010) includes so-called long-distance dispersal (LDD) events. There are essentially two main causes for LDD events: transport due to antrropic activities, and transport with the wind of individuals that ventured above the forest canopy (particularly on occasion of storms). Transport processes can easily produce patchiness (see, for example, the case of zebra mussels carried downstream a river: Mari et al., 2009). In addition, in our case, they are also completely random and unpredictable: while the outcome of each LDD event could be forecast by a model, after its occurrence, and provided the availability of sufficient observational data, the occurrence of the event itself can not be forecast. Because our model does not (yet) have the ambition of being an operational one, but it is meant to uncover and elucidate some ecological processes in the interaction between *D. kuriphilus* and *T. sinensis*, we have, for the moment, refrained from including LDDs into it.

However, we do not expect LDDs to change the overall picture that has emerged about the likeliness of achieving biological control of *D. kuriphilus* with *T. sinensis*. In fact, a random LDD event involving *D. kuriphilus* may have a good chance of carrying the pest in a region where it is absent, thus creating a new hotspot of infestation. On the other hand, a random LDD event involving *T. sinensis* can only contribute to the effectiveness of biological control if the parasitoid lands in a region populated by the pest and devoid of the parasitoid. If it lands in an area where the pest is absent, the event has no effect. If it lands close to a parasitoid sweeping wave, that region would have been swept in any case, and thus the effect is also limited. Thus, it seems reasonable to assume that LDDs do not improve the chances of achieving control, and, if anything, they diminish them. Overall the message remains the same: biological control of *D. kuriphilus* with *T. sinensis* may be a viable option, but only if one is prepared to carefully track the distribution of both species and to suppress any new hotspots (or recolonization waves) with further releases of the parasitoid.

5. Appendix

5.1. Approximations of the space-independent solution of the gall wasp equations

Let us define $y_n(t) = \log(1 - v_n(t))$. Substituting in (11) we obtain

$$\begin{cases} \dot{u}_n(t) = -\mu(1 + e^{y_n(t)})u_n(t) + v_{n-1}(1) \\ \dot{y}_n(t) = -E_D\mu u_n(t) \\ u_n(0) = 0 \\ y_n(0) = 0 \end{cases} \quad (31)$$

Observe that in (31), because the egg density v_n obeys $0 \leq v_n < 1$, then $-\infty < y \leq 0$, and thus it is $1 < 1 + e^{y_n(t)} \leq 2$. This implies that

$$\frac{v_{n-1}(1)}{\mu}(1 - e^{-\mu t}) > u_n(t) \geq \frac{v_{n-1}(1)}{2\mu}(1 - e^{-2\mu t}) \quad (32)$$

Using these inequalities in the second of (31) and from $v_n(t) = 1 - e^{y_n(t)}$, follow the inequalities

$$1 - e^{-\frac{E_D}{\mu}(e^{-\mu t} + \mu t - 1)v_{n-1}(1)} > v_n(t) > 1 - e^{-\frac{E_D}{4\mu}(e^{-2\mu t} + 2\mu t - 1)v_{n-1}(1)}. \quad (33)$$

By evaluating the above expression at time $t = 1$ one finds that the year-over-year evolution of the end of season egg density $v_n(1)$ may be approximated by the map (12) with the constants (13).

Note that the approximation from below, obtained by choosing k_- in (13), is very accurate if the density of eggs laid in the previous year is low. In fact, by taking $v_{n-1}(1)$ arbitrarily close to zero it is possible, from (32), to keep $u_n(t)$ as small as one wishes, for all $t \in [0, 1]$, and, from the second of (31) also $y_n(t)$ may be kept as close to zero as one wishes, for all $t \in [0, 1]$. Therefore, the quantity $1 + e^{y_n(t)}$ may be kept arbitrarily close to 2, which is the value used

by the approximation from below. Conversely, if $v_{n-1}(1)$ is close to one, and the product $E_D\mu$ is much larger than one, then $1 + e^{y_n(t)}$ will rapidly approach the value 1. Therefore, we expect the approximation from above to be more accurate at high densities of eggs laid in the previous year.

5.2. Exact space-independent solution of the equations for *T. sinensis*

By imposing no-flux boundary conditions on p_n , assuming that $\nabla v_{n-1} = \nabla q_{n-1} = 0$, the equations (18) and the conditions (19) become

$$\begin{cases} \dot{p}_n(t) = -\tau^{-1}(v_{n-1}(1) - q_n(t))p_n(t) \\ \dot{q}_n(t) = E_T\tau^{-1}(v_{n-1}(1) - q_n(t))p_n(t) \\ p_n(0) = q_{n-1}(\eta\tau) \\ q_n(0) = 0 \end{cases}. \quad (34)$$

Dividing the first by the second we have

$$\dot{p}_n = -\frac{1}{E_T}\dot{q}_n,$$

and thus, by integration and using the initial conditions, we find

$$p_n(q_n(t)) = -\frac{q_n(t)}{E_T} + q_{n-1}(\eta\tau).$$

Substituting this expression in the second of the equations (34) we obtain a first-order, autonomous equation for q_n which yields the following solution

$$\begin{cases} \begin{cases} p_n(t) = \frac{\bar{q}_{n-1}(E_T\bar{q}_{n-1} - \bar{v}_{n-1}) \exp\left(\frac{t}{\tau}(E_T\bar{q}_{n-1} - \bar{v}_{n-1})\right)}{\bar{q}_{n-1}E_T \exp\left(\frac{t}{\tau}(E_T\bar{q}_{n-1} - \bar{v}_{n-1})\right) - v_{n-1}^*} \\ q_n(t) = \frac{\bar{v}_{n-1}\bar{q}_{n-1}E_T(1 - \exp\left(\frac{t}{\tau}(E_T\bar{q}_{n-1} - \bar{v}_{n-1})\right))}{\bar{v}_{n-1} - \bar{q}_{n-1}E_T \exp\left(\frac{t}{\tau}(E_T\bar{q}_{n-1} - \bar{v}_{n-1})\right)} \end{cases}, & E_T\bar{q}_{n-1} \neq \bar{v}_{n-1} \\ \begin{cases} p_n(t) = \frac{\bar{v}_{n-1}\tau}{E_T(\bar{v}_{n-1}t + \tau)} \\ q_n(t) = \frac{\bar{v}_{n-1}^2 t}{\bar{v}_{n-1}t + \tau} \end{cases}, & E_T\bar{q}_{n-1} = \bar{v}_{n-1} \end{cases}$$

where, for brevity, we have defined the shorthands $\bar{q}_{n-1} = q_{n-1}(\eta\tau)$, $\bar{v}_{n-1} = v_{n-1}(1)$. It can be verified, by expanding the exponentials in power series, that the above solution is a smooth function of the quantity $E_T\bar{q}_{n-1} - \bar{v}_{n-1}$.

5.3. Mathematical properties of the space-independent map

5.3.1. Boundedness of the global dynamics

The map (23), formally, does not allow for the extinction of either species. Specifically, the map has the property that, if $E_T, \eta, k > 0$ and $0 < v_n, q_n$ then $0 < v_{n+1}, q_{n+2} < 1$.

This assert becomes apparent by rewriting the map in the following form

$$\begin{cases} q_{n+1} = \begin{cases} \left(\frac{1 - e^{\eta(E_T q_n - v_n)}}{\frac{v_n}{E_T q_n} - e^{\eta(E_T q_n - v_n)}} \right) v_n, & E_T q_n \neq v_n \\ \left(\frac{v_n}{\eta^{-1} + v_n} \right) v_n, & E_T q_n = v_n \end{cases} \\ v_{n+1} = 1 - e^{-k(v_n - q_{n+1})} \end{cases} \quad (35)$$

It is straightforward to verify that

$$0 < [1 - \exp(\eta(E_T q_n - v_n))] [v_n E_T^{-1} q_n^{-1} - \exp(\eta(E_T q_n - v_n))]^{-1} < 1$$

both if $E_T q_n < v_n$ and if $E_T q_n > v_n$. Obviously, it is also

$$0 < v_n [\eta^{-1} + v_n]^{-1} < 1,$$

which is relevant in the case $E_T q_n = v_n$. Therefore, from the equation for q_{n+1} in (35) we have $0 < q_{n+1} < v_n$. Using this inequality in the equation for v_{n+1} in (35) we have $0 < v_{n+1} < 1$, and, therefore $0 < q_{n+2} < v_{n+1} < 1$.

5.3.2. Nullclines and the coexistence fixed point

We defined v -nullcline as the set of pairs (v_n, q_{n+1}) such that $v_{n+1} = v_n$. From the second equation in (23), we find that the v -nullcline has the following explicit expression

$$q_{n+1}(v_n) = v_n + \frac{1}{k} \log(1 - v_n) \quad (36)$$

whose graph is the red line in the right panel of Figures 3, 4, 5. A simple calculation shows that if (v_n, q_{n+1}) is above the v -nullcline, then $v_{n+1} < v_n$, and if it is below, then $v_{n+1} > v_n$. If $k > 1$ then the v -nullcline has a maximum at

$$v_{mx} = \frac{k-1}{k}, \quad q_{mx} = \frac{k-1-\log(k)}{k}. \quad (37)$$

It also has a zero at $v_n = 0$, and at a value larger than v_{mx} and smaller than 1, which does not have a simple explicit expression, and corresponds to the non-zero fixed point of Skellam's map (12).

Analogously we defined the q -nullcline as the set of pairs (v_n, q_n) such that $q_{n+1} = q_n$. The q -nullcline has an obvious branch which is $q_n = 0$. From the first equation in (23), if $v_n, q_n \neq 0$ and $E_T q_n \neq v_n$, we have the following implicit definition of the q -nullcline

$$\frac{v_n - q_n}{v_n} e^{\eta(E_T q_n - v_n)} = \frac{E_T - 1}{E_T}. \quad (38)$$

In the case $E_T q_n = v_n > 0$, it is straightforward to verify from (23) that only the point $(v_n, q_n) = (\eta^{-1}(E_T - 1)^{-1}, \eta^{-1}(E_T - 1)^{-1} E_T^{-1})$ belongs to the q -nullcline, shown as the green curve in the right panel of Figures 3, 4, 5. If $q_n \rightarrow 0$, the q -nullcline tends to the value

$$v_z = \frac{1}{\eta} \log\left(\frac{E_T}{E_T - 1}\right). \quad (39)$$

Note that, if $E_T > 1$ then the right-hand side of (38) is larger than 0 and smaller than 1. Thus, for fixed η and $v_n \neq v_z$, if $E_T \rightarrow \infty$ either there is no solution to (38), or $q_n \rightarrow v_n$ from below. This observation suggests that for realistic values of the parameters (that is η not much smaller than 1 and E_T quite larger than

10), taking $q_n \approx v_n$ for $v_n > v_z$ should give a reasonably good approximation of the q -nullcline.

With respect to the new variable $z = q_n/v_n$, the implicit expression (38) may be made explicit, and one finds

$$v_n(z) = \frac{1}{\eta(E_T z - 1)} \log \left(\frac{E_T - 1}{E_T - E_T z} \right) \quad (40)$$

Note that $0 < z < 1$ because $q_n = q_{n+1} < v_n$. It can be checked that this is a strictly growing function of z , which is smooth even at $z = E_T^{-1}$. (In order to verify the positive sign of the derivative the identity $\log(x) \leq x - 1$ can be useful.) Thus the minimum of this function is attained in the limit $z \rightarrow 0$, where $v_n \rightarrow v_z$: for $v_n < v_z$ the equation (38) has no solution. We also observe that, because $v'_n(z) > 0$, to each value of z corresponds a unique value of $q_n(z) = z v_n(z)$. Therefore, calling ζ the inverse function of (40), we have that the equation (38) implicitly defines a unique continuous function $q_n(v_n) = v_n \zeta(v_n)$ of v_n , that we shall call the non-zero branch of the q -nullcline, and that $q'_n(v_n) > 0$, as depicted by the green line in the right panel of Figures 3, 4, 5.

From the first equation in (42) below, (see also the surrounding discussion) it is clear that, for states not belonging to the q -nullcline having arbitrarily small q_n , if $v_n < v_z$ then $q_{n+1} < q_n$, and if $v_n > v_z$ then $q_{n+1} > q_n$. Thus, since the non-zero branch of the q -nullcline is unique, by the theorem of the persistence of sign, if a state (v_n, q_n) lies on the left of the q -nullcline, then $q_{n+1} < q_n$; if it lies on the right, then $q_{n+1} > q_n$.

Fixed points are the intersection of the v -nullcline and of the q -nullcline. There is always the fixed point $(v_n, q_n) = (0, 0)$. If $k > 1$ then there is also the fixed point $(v_n, q_n) = (v^*, 0)$ where v^* is the non-zero fixed point of Skellam's map (12).

If $k > 1$ and $v_z < v^*$, then the non-zero branch of the q -nullcline (which is a growing function of v_n) must cross at at least one point the v -nullcline (which is positive and has a zero at $v_n = 0$ and a zero at $v_n = v^*$). We call this is a *coexistence* fixed point, because both v_n and q_n are larger than 0. Note that, except for unrealistically low values of k , the non-zero fixed point of Skellam's map is very close to one. Thus, an approximate criterion for the existence of a coexistence fixed point is $v_z < 1$. Using the expression (39) and the definition of E_T (see Table 2), setting $v_z = 1$ one obtains the approximate threshold (24).

We have ample numerical evidence, corroborated by asymptotic results, that there is only one coexistence fixed point, although we cannot exclude that for some finely-tuned value of the parameters more than one coexistence fixed point could exist.

In the realistic range of parameters, a very rough approximation of the position of the coexistence fixed point may be obtained by approximating the v -nullcline as

$$q_{n+1}(v_n) \approx \left(1 - \frac{1}{k}\right) v_n$$

and the q -nullcline as the straight line connecting the points

$$(v_n, q_n) = (\eta^{-1}(E_T - 1)^{-1}, \eta^{-1}(E_T - 1)^{-1}E_T^{-1}) \quad \text{and} \quad (v_n, q_n) = (1, 1).$$

Looking for the intersection of these straight lines we find

$$\begin{cases} v_c = \frac{k(E_T - 1)}{E_T[\eta(E_T - 1)^{-1}] + k(E_T - 1)}, \\ q_c = \frac{(k-1)(E_T - 1)}{E_T[\eta(E_T - 1)^{-1}] + k(E_T - 1)}. \end{cases} \quad (41)$$

More accurate approximations of the q -nullcline (and thus of the coexistence fixed point) can be worked out by evaluating (40) at the values z_m such that

$$\frac{E_T - 1}{E_T - E_T z_m} = e^{\eta E_T / m}$$

for distinct values of the arbitrary parameter m . This yields explicit expressions of points $(v_n(z_m), q_n(z_m))$ lying on the q -nullcline among which it is possible to interpolate with any standard method.

5.3.3. Cycles around the fixed point

The cyclic dynamics generated by the map (23) may be qualitatively understood through the following argument. For small q_n , the map (23) becomes, at leading order

$$\begin{cases} q_{n+1} = (1 - e^{-\eta v_n}) E_T q_n + O(q_n^2) \\ v_{n+1} = (1 - e^{-k v_n}) + O(v_n q_n). \end{cases} \quad (42)$$

Let us assume that initially v_n is also very small. Thus the egg density of *T. sinensis* decreases from one year to the next as long as $(1 - e^{-\eta v_n}) < E_T^{-1}$, that is, until $v_n < v_z$ (see eq. 39). However, *D. kuriphilus* is at leading order decoupled from its parasitoid, and its egg density obeys Skellam's map (12). Therefore, assuming $k > 1$, v_n will grow with n until it approaches the non-zero fixed point of Skellam's map, which, for realistic values of k , has a numerical value very close to 1. At this point the egg density of *T. sinensis* will be growing in time, but it may require several years before reaching an $O(1)$ magnitude. Thus, starting from very small values of v_n and q_n , we have that the sequence of states, seen in a diagram q_n vs v_n , as in the right panel of Figure 5, first moves horizontally (v_n growing, q_n very close to 0) and then vertically (v_n very close to 1, q_n growing). When q_n reaches $O(1)$ the approximation (42) no longer applies, and it is convenient to rewrite the map (23) as (35), and then (assuming $E_T q_n \neq v_n$) as

$$\begin{cases} q_{n+1} = \left(\frac{e^{-\eta(E_T q_n - v_n)} - 1}{\frac{v_n}{E_T q_n} e^{-\eta(E_T q_n - v_n)} - 1} \right) v_n \\ v_{n+1} = 1 - e^{-k(v_n - q_{n+1})} \end{cases} \quad (43)$$

With $q_n = O(1)$ for large (realistic) values of E_T the parenthesis appearing in the first equation approaches 1. Thus we have $q_{n+1} \approx v_n$, which leads to a

cancellation in the exponent appearing in the second equation, causing a sharp drop in the value of v_{n+1} with respect to v_n . Thus the system jumps from a state ($v_n \approx 1$, $q_n = O(1)$) close to right edge of Figure 5 (right panel) to a state close to its upper edge ($v_{n+1} \approx O(1)$, $q_{n+1} \approx 1$) or, more often, depending on the exact value of q_n , to a state close to its upper-left corner ($v_{n+1} \ll 1$, $q_{n+1} \approx 1$). The next year, since $q_{n+1} \approx 1$, the cancellation occurs again, and the further drop in the value of *D. kuripilus*' egg density is as large as ten orders of magnitude, with the parameters of Figure 5. Thus, in the turn of just two years, *T. sinensis* wipes out almost all the population of *D. kuripilus*, and, consequently, its own, because of the constraint $q_{n+1} < v_n$. Then the cycle starts again.

Note that the cycles need not be exactly periodic. In fact, the intervals of exponential growth of q_n and the subsequent cancellation events could even produce a chaotic dynamics (however we did not investigate this issue). More importantly, small differences in the value of q_n before the cancellation events can make a large difference in the number of orders of magnitude lost after the events, and thus in the number of years needed to re-grow up to $O(1)$.

References

- Abe Y., Melika G., Stone G. N. (2007) The diversity and phylogeography of cynipid gallwasps (Hymenoptera, Cynipidae) of the Eastern Palearctic and their associated communities. *Oriental Insects* 41:169–212.
- Alma A., Ferracini C., Sartor C., Ferrari E., Botta R. (2014) Il cinipide orientale del castagno: lotta biologica e sensibilità varietale. *Italus Hortus* 21(3):15–29.
- Balkovsky E., Shraiman B. I. (2002) Olfactory search at high Reynolds number. *PNAS* 99(20):12589–12593.
- Battisti A., Benvegnù I., Colombari F., Haack R. A. (2014) Invasion by the chestnut gall wasp in Italy causes significant yield loss in *Castanea sativa* nut production. *Agric. Forest. Entomol.* 16(1): 75–79.
- Borowiec N., Thaon M., Brancaccio L., Warot S., Vercken E., Fauvergue X., Ris N., Malausa J. C. (2014) Classical biological control against the chestnut gall wasp *Dryocosmus kuriphilus* (Hymenoptera, Cynipidae) in France. *Plant Prot. Q.* 29(1):7–10.
- Bosio G., Armando M., Moriya S. (2013). Verso il controllo biologico del cinipide del castagno. *Informatore Agrario* 4(14):60–64.
- Bounous G. (2014) Il castagno: risorsa multifunzionale in Italia e nel mondo. Edagricole, Bologna.
- Brännström Å., Sumpter D. J. T. (2005). The role of competition and clustering in population dynamics. *Proc. R. Soc. B* 272: 2065–2072.

- Brussino G., Bosio G., Baudino M., Giordano R., Ramello F., Melika G., (2002) Pericoloso insetto esotico per il castagno europeo. *Informatore Agrario*, 58(37):59–61.
- Cooper W. R., Rieske L. K. (2007) Community associates of an exotic gall-maker, *Dryocosmus kuriphilus* (Hymenoptera: Cynipidae), in Eastern North America. *Ann. Entomol. Soc. Am.* 100(2):236-244.
- Cooper W. R., Rieske L. K. (2010). Gall Structure Affects Ecological Associations of *Dryocosmus kuriphilus* (Hymenoptera: Cynipidae). *Environ. Entomol.* 39(3):787–797.
- Cho D. Y., Lee S. O. (1963) Ecological studies on the chestnut gall wasp, *Dryocosmus kuriphilus* Yasumatsu, and observations on the damages of the chestnut trees by its insect. *Kor. J. Plant Protect.* 2:47–54.
- del-Castillo-Negrete D., Carreras B. A., Lynch V. E. (2003) Front dynamics in reaction-diffusion systems with Levy flights: a fractional diffusion approach. *Physical Review Letters* 91(1): 018302.
- EFSA Panel on Plant Health (PLH) (2010) Risk assessment of the oriental chestnut gall wasp, *Dryocosmus kuriphilus* for the EU territory on request from the European Commission. *EFSA J* 8:1619
- EPPO (2005) Data sheets on quarantine pests-*Dryocosmus kuriphilus*. *EPPO Bull* 35:422–424.
- EPPO (2013) First report of *Dryocosmus kuriphilus* in Austria (2013/140, First report of *Dryocosmus kuriphilus* in Germany 2013/141, *Dryocosmus kuriphilus* found in Hungary 2013/142. *Eppo Reporting service*, No. 7, pp. 3–4.
- EPPO (2015a) First report of *Dryocosmus kuriphilus* in the United Kingdom. *Eppo Reporting service*, No. 6, pp. 2.
- EPPO (2015b) *Dryocosmus kuriphilus* found again in the Netherlands 2015/128. *Eppo Reporting Service no.7* p. 3.
- Ferracini C., Ferrari E., Saladini M. A., Pontini M., Corradetti M., Alma A. (2015a) Non-target host risk assessment for the parasitoid *Torymus sinensis*. *BioControl*, in press. DOI:10.1007/s10526-015-9676-1.
- Ferracini C., Gonella E., Ferrari E., Saladini M. A., Picciau L., Tota F., Pontini M., Alma A. (2015b) Novel insight in the life cycle of *Torymus sinensis*, biocontrol agent of the chestnut gall wasp. *BioControl*, 60:583–594.
- Gardiner C. W.. (2004) *Handbook of Stochastic Methods*. III edition. Springer-Verlag Berlin Heidelberg.

- Germinara G. S., De Cristofaro A., Rotundo G. (2011) Chemical Cues for Host Location by the Chestnut Gall Wasp, *Dryocosmus kuriphilus*. *J. Chem. Ecol.* 37:49–56.
- Gibbs M., Schönrogge K., Alma A., Melika G., Quacchia A., Stone G. N., Aebi A. (2011) *Torymus sinensis*: a viable management option for the biological control of *Dryocosmus kuriphilus* in Europe? *BioControl* 56:527–538.
- Graziosi I., Santi F. (2008) Chestnut gall wasp (*Dryocosmus kuriphilus*): spreading in Italy and new records in Bologna province. *Bull. Insectol.* 61(2):343–348.
- Graziosi I., Rieske L. K. (2013) Response of *Torymus sinensis*, a parasitoid of the gallforming *Dryocosmus kuriphilus*, to olfactory and visual cues. *Biological Control* 67:137–142.
- Graziosi I., Rieske L. K. (2014) Potential fecundity of a highly invasive gall maker, *Dryocosmus kuriphilus* (Hymenoptera: Cynipidae). *Environmental Entomology* 43(4):1053–1058.
- Hassell M., P., Comins H. N., May R. M. (1991) Spatial structure and chaos in insect population dynamics. *Nature* 353(6341):255–258.
- Henneman M. L., Dyreson E. G., Takabayashi J., Raguso R. A. (2002) Response to walnut olfactory and visual cues by the parasitic wasp *Diachasmimorpha juglandis*. *J. Chem. Ecol.* 28(11):2221–2244.
- Huber J. T., Read J. (2012) First record of the oriental chestnut gall wasp, *Dryocosmus kuriphilus* Yasumatsu (Hymenoptera: Cynipidae), Canada. *J. Entomol. Soc. Ont.* 143:125–128.
- Huffaker C. B. (1958) Experimental Studies on Predation: Dispersion Factors and Predator–Prey Oscillations. *Hilgardia: A Journal of Agricultural Science* 27:795–834.
- Johansson F. et al. (2013) Mpmath: a Python library for arbitrary-precision floating-point arithmetic (version 0.18). <http://mpmath.org/>
- Kamijo K. (1982) Two new species of *Torymus* (Hymenoptera, Torymidae) reared from *Dryocosmus kuriphilus* (Hymenoptera, Cynipidae) in China and Korea. *Kontyû* 50:505–510.
- Kato K, Hijii N (1997) Effects of gall formation by *Dryocosmus kuriphilus* Yasumatsu (Hymenoptera: Cynipidae) on the growth of chestnut trees. *J. Appl. Entomol.* 121:9–15.
- Mari L., Casagrandi R., Pisani M. T., Pucci E., Gatto, M. (2009). When will the zebra mussel reach Florence? A model for the spread of *Dreissena polymorpha* in the Arno water system (Italy). *Ecohydrology*, 2(4):428–439.

- Matošević D., Quacchia A., Kriston E., Melika G., (2014). Biological control of the invasive *Dryocosmus kuriphilus* (Hymenoptera: Cynipidae) - an overview and the first trials in Croatia. *South-east European Forestry*, 5(1): 3–12.
- May R. M., McLean A. R., (2007). *Theoretical ecology: principles and applications*. Oxford University Press, III ed, Oxford (UK).
- Moriya S., Inoue K., Ôtake A., Shiga M., Mabuchi M. (1989) Decline of the chestnut gall wasp population, *Dryocosmus kuriphilus* Yasumatsu (Hymenoptera: Cynipidae) after the establishment of *Torymus sinensis* Kamijo (Hymenoptera: Torymidae). *Appl Entomol Zool* 24:231–233.
- Moriya S., Shiga M., Adachi I. (2003) Classical biological control of the chestnut gall wasp in Japan. In: Van Driesche R. G. (ed) *Proceedings of the 1st International Symposium on Biological Control of Arthropods*. USDA Forest Service, Washington.
- Murakami Y., Umeya K., Oho N. (1977) A preliminary introduction and released of a parasitoid (Chalcidoidea, Torymidae) of the chestnut gall wasp *Dryocosmus kuriphilus* Yasumatsu. *Jpn J Appl Entomol Zool* 21:197–203.
- Murakami Y., Ao H. B., Chang C. H. (1980) Natural enemies of the chestnut gall wasp in Hopei Province, China (Hymenoptera: Chalcidoidea). *Appl. Entomol. Zool.* 15:184–186.
- Murakami Y. (1981) The parasitoids of *Dryocosmus kuriphilus* Yasumatsu (Hymenoptera: Cynipidae) in Japan and the introduction of a promising natural enemy from China (Hymenoptera: Chalcidoidea). *J. Fac. Agric. Kyushu Univ.* 25:167–174.
- Murakami Y. and Gyoutoku Y. (1991) Colonization of the imported *Torymus (Syntomaspis) sinensis* Kamijo (Hymenoptera: Torymidae) parasitic on the chestnut gall wasp (Hymenoptera: cynipidae). (5) Mortality of *Torymus* spp. by native facultative hyperparasitoids. *Proceedings of the Association for Plant Protection of Kyushu* 37: 194–197.
- Murakami Y., Gyoutoku Y. (1995) A delayed increase in the population of an imported parasitoid, *Torymus (Syntomaspis) sinensis* (Hymenoptera: Torymidae) in Kumamoto, Southwestern Japan. *Appl Entomol Zool* 30:215–224.
- Murakami Y., Toda S., Gyoutoku Y. (2001) Colonization of imported *Torymus (Syntomaspis) sinensis* Kamijo (Hymenoptera: Torymidae) parasitic on the chestnut gall wasp (Hymenoptera: Cynipidae). Success in the eighteenth year after release in Kumamoto. *Proc. Assoc. Pl. Prot. Kyushu* 47:132–134.
- Murray J. D. (2007) *Mathematical Biology I. An Introduction*. Springer, Berlin, 3rd ed.

- NPPO The Netherlands (2013) Follow-up pest report *Dryocosmus kuriphilus*. Confirmation of eradication. October 2013 Pest Report - The Netherlands. Wageningen, The Netherlands: NPPO The Netherlands, 1.
- Ôtake A. (1980) Chestnut gall wasp, *Dryocosmus kuriphilus* Yasumatsu (Hymenoptera: Cynipidae): a preliminary study on trend of adult emergence and some other ecological aspects related to the final stage of its life cycle. *Appl. Entomol. Zool.* 15:96–105.
- Piao C. S., Moriya S. (1992) Longevity and oviposition of *Torymus sinensis* Kamiyo and two strains of *T. beneficus* Yasumatsu et Kamiyo (Hymenoptera: Torymidae). *Jap. J. Appl. Entomol. Zool.* 36:113–118.
- Quacchia A., Moriya S., Bosio G., Scapin G., Alma A. (2008) Rearing, release and settlement prospect in Italy of *Torymus sinensis*, the biological control agent of the chestnut gall wasp *Dryocosmus kuriphilus*. *BioControl* 53:829–839.
- Quacchia A., Ferracini C., Nicholls J. A., Piazza E. Saladini M. A., Tota F., Melika G., Alma A. (2013) Chalcid parasitoid community associated with the invading pest *Dryocosmus kuriphilus* in north-western Italy. *Insect conservation and diversity* 6(2):114–123.
- Rieske L. K. (2007) Success of an exotic gallmaker, *Dryocosmus kuriphilus*, on chestnut in the USA: a historical account. *EPPPO Bull* 37:172–174.
- Skellam, J. G. (1951) Random dispersal in theoretical populations. *Biometrika* 38:196–218.
- Vandermeer J. H. and Goldberg D. E. (2013) *Population Ecology: first principles*. Princeton University Press, II edition, Princeton (NJ), USA.
- Viswanathan G. M., Raposo E. P., da Luz M. G. E. (2008) Lévy flights and superdiffusion in the context of biological encounters and random searches. *Physics of Life Reviews* 5(3):133–150.